



Reprint 2016-8

Transient Climate Impacts for Scenarios of Aerosol Emissions from Asia: A Story of Coal versus Gas

Benjamin S. Grandey, Haiwen Cheng, Chien Wang

Reprinted with permission from *Journal of Climate*, 29(8): 2849-2867.

© 2016 American Meteorological Society

The MIT Joint Program on the Science and Policy of Global Change combines cutting-edge scientific research with independent policy analysis to provide a solid foundation for the public and private decisions needed to mitigate and adapt to unavoidable global environmental changes. Being data-driven, the Joint Program uses extensive Earth system and economic data and models to produce quantitative analysis and predictions of the risks of climate change and the challenges of limiting human influence on the environment—essential knowledge for the international dialogue toward a global response to climate change.

To this end, the Joint Program brings together an interdisciplinary group from two established MIT research centers: the Center for Global Change Science (CGCS) and the Center for Energy and Environmental Policy Research (CEEPR). These two centers—along with collaborators from the Marine Biology Laboratory (MBL) at

Woods Hole and short- and long-term visitors—provide the united vision needed to solve global challenges.

At the heart of much of the program's work lies MIT's Integrated Global System Model. Through this integrated model, the program seeks to discover new interactions among natural and human climate system components; objectively assess uncertainty in economic and climate projections; critically and quantitatively analyze environmental management and policy proposals; understand complex connections among the many forces that will shape our future; and improve methods to model, monitor and verify greenhouse gas emissions and climatic impacts.

This reprint is intended to communicate research results and improve public understanding of global environment and energy challenges, thereby contributing to informed debate about climate change and the economic and social implications of policy alternatives.

—Ronald G. Prinn and John M. Reilly,
Joint Program Co-Directors

Transient Climate Impacts for Scenarios of Aerosol Emissions from Asia: A Story of Coal versus Gas

BENJAMIN S. GRANDEY AND HAIWEN CHENG

Center for Environmental Sensing and Modeling, Singapore–MIT Alliance for Research and Technology, Singapore

CHIEN WANG⁺

Center for Global Change Science, Massachusetts Institute of Technology, Cambridge, Massachusetts

(Manuscript received 31 July 2015, in final form 5 January 2016)

ABSTRACT


Fuel usage is an important driver of anthropogenic aerosol emissions. In Asia, it is possible that aerosol emissions may increase if business continues as usual, with economic growth driving an increase in coal burning. But it is also possible that emissions may decrease rapidly as a result of the widespread adoption of cleaner technologies or a shift toward noncoal fuels, such as natural gas. In this study, the transient climate impacts of two aerosol emissions scenarios are investigated: a representative concentration pathway 4.5 (RCP4.5) control, which projects a decrease in anthropogenic aerosol emissions, and a scenario with enhanced anthropogenic aerosol emissions from Asia. A coupled atmosphere–ocean configuration of the Community Earth System Model (CESM), including the Community Atmosphere Model, version 5 (CAM5), is used. Three sets of initial conditions are used to produce a three-member ensemble for each scenario. Enhanced Asian aerosol emissions are found to exert a large cooling effect across the Northern Hemisphere, partially offsetting greenhouse gas–induced warming. Aerosol-induced suppression of the East Asian and South Asian summer monsoon precipitation occurs. The enhanced Asian aerosol emissions also remotely impact precipitation in other parts of the world. Over Australia, austral summer monsoon precipitation is enhanced, an effect associated with a southward shift of the intertropical convergence zone, driven by the aerosol-induced cooling of the Northern Hemisphere. Over the Sahel, West African monsoon precipitation is suppressed, likely via a weakening of the West African westerly jet. These results indicate that fuel usage in Asia, through the consequent aerosol emissions and associated radiative effects, might significantly influence future climate both locally and globally.

1. Introduction

Coal is a common fuel across much of Asia. In both China and India, it is the dominant source of sulfur dioxide (SO₂) (Lu et al. 2011), a precursor of sulfate aerosol. Coal, alongside biofuel burning, is also one of

the two largest sources of black carbon (BC) aerosol in these countries. In both countries, SO₂ and BC emissions have increased between 1996 and 2010 (Lu et al. 2011). For example, SO₂ emissions in India have increased by 70% over this 14-yr period, driven by increasing energy consumption.

Economic growth may continue to drive an increasing emission trend, especially as coal usage is still increasing (Steckel et al. 2015). On the other hand, policies promoting the use of cleaner technologies have the potential to reduce emissions; Zhao et al. (2010) found that SO₂ scrubbers [wet flue gas desulfurization (FGD) systems] can remove up to 95% of SO₂ at coal-fired power plants in China, and Zhi et al. (2009) suggest that household BC emissions from coal could be reduced by up to 98% through the use of efficient briquettes and improved stoves. Emissions may also be reduced through the use of alternative fuels such as natural gas;

 Denotes Open Access content.

 Supplemental information related to this paper is available at the Journals Online website: <http://dx.doi.org/10.1175/JCLI-D-15-0555.s1>.

⁺ Additional affiliation: Center for Environmental Sensing and Modeling, Singapore–MIT Alliance for Research and Technology, Singapore.

Corresponding author address: Benjamin S. Grandey, 1 CREATE Way, #09-03 CREATE Tower, Singapore 138602, Singapore.
E-mail: benjamin@smart.mit.edu

DOI: 10.1175/JCLI-D-15-0555.1

the U.S. Energy Information Administration (2013) estimates that China has the largest shale gas reserves in the world. In light of the economic, technological, and policy uncertainties, future emissions trends of anthropogenic SO₂ and BC remain highly uncertain.

In addition to being a public health concern, atmospheric aerosols such as sulfate and BC impact climate. In this study, we explore how the climate might respond to different scenarios of anthropogenic sulfur and BC emissions from Asia. Before describing our modeling experiments, we provide an introduction to some earlier studies that have investigated possible aerosol effects on climate.

It is well established that aerosols can scatter or absorb incoming solar radiation (Haywood and Boucher 2000), causing a cooling at Earth's surface. Absorbing aerosols, such as BC, also heat the atmosphere when they absorb solar radiation, potentially affecting clouds (Ackerman 2000). Many aerosols, such as sulfate, act as cloud condensation nuclei. Therefore, changes in aerosol concentrations and properties may impact cloud microphysical properties such as droplet size (Twomey 1974, 1977) and processes such as precipitation formation (Albrecht 1989). Establishing a climatically meaningful understanding of interactions between aerosols, clouds, and precipitation remains a difficult but important task (Stevens and Feingold 2009; Tao et al. 2012).

These aerosol effects may impact large-scale circulations in the atmosphere. Absorbing aerosols, such as BC, may play a particularly important role (Wang 2013). For example, Chung et al. (2002) found that absorbing aerosols impact South Asian precipitation during the dry monsoon season (November–May). Lau et al. (2006) explained South Asian precipitation changes using an “elevated heat pump” hypothesis: during the premonsoon season, atmospheric heating near the Tibetan Plateau causes summer monsoon precipitation to arrive earlier and become more intense. Wang et al. (2009) used moist static energy to provide a thermodynamic perspective of why absorbing aerosol may cause early monsoon precipitation to shift northward. Lee et al. (2013) demonstrated that nonlinear interactions between aerosol-induced atmospheric heating and surface cooling are important.

During the summer monsoon season (June–September), much of the absorbing BC aerosol is removed from the atmosphere via wet scavenging. However, Ramanathan et al. (2005) demonstrated that premonsoon BC impacts on sea surface temperatures (SSTs) may persist into the monsoon season. Reduced SSTs lead to a reduction in monsoon precipitation over India, as was corroborated by Meehl et al. (2008). Similarly, Lee and Wang (2015, p. 6626) found that “soil

water storage is found to retain the effects of premonsoonal forcing into succeeding months, resulting in monsoonal central India drying.”

Recent studies have highlighted that nonabsorbing aerosols, such as sulfate, may also have significant impacts on the South Asian monsoon. Bollasina et al. (2011) found that anthropogenic aerosols can weaken the tropical meridional circulation, leading to a precipitation reduction in central-northern India. In contrast to earlier studies, they suggested that indirect effects of sulfate aerosol were primarily responsible.

Aerosol–monsoon interactions are probably not limited to South Asia. At the very least, aerosols appear to impact the monsoon in East Asia. Menon et al. (2002) found that absorbing aerosols affect the precipitation distribution in China. The elevated heat pump hypothesis (Lau et al. 2006) suggests that the absorbing aerosols would cause East Asian precipitation to move northwestward, reducing precipitation over East Asia. Gu et al. (2006) provided further evidence that absorbing aerosols may cause East Asian precipitation to move inland. Jiang et al. (2013) found that anthropogenic aerosols may reduce precipitation in northern China and increase precipitation in southern China, with both BC and sulfate playing important roles. Liu et al. (2011) suggested that anthropogenic aerosols may reduce summer precipitation in China via indirect effects, increased atmospheric stability, and a weakening of the East Asian monsoon. Guo et al. (2013) found that the East Asian monsoon is particularly sensitive to aerosol-induced surface cooling during September, with sulfate potentially playing a larger role than BC in the suppression of precipitation. If anthropogenic aerosol emissions decrease in the future, the precipitation impacts in East Asia and South Asia would likely reverse (Levy et al. 2013).

Aerosol sources from outside Asia may also contribute to aerosol–monsoon interactions within Asia. Cowan and Cai (2011) suggested that non-Asian aerosols intensify the impact of Asian aerosols on the Asian monsoon. Ganguly et al. (2012) suggested that non-Asian aerosol sources are important during the latter part of the Asian monsoon, although local aerosol sources dominate earlier on. Bollasina et al. (2014) found that the lower-tropospheric circulation in South Asia may actually be affected more by remote aerosol sources than by local aerosol sources.

Conversely, Asian aerosol emissions may remotely affect regions in other parts of the world. For example, Menon et al. (2002) stated, “The BC absorption in China and India causes a significant warming (>0.5 K) in the Sahara Desert region and in west and central Canada, despite the fixed SST” (p. 2250). Teng et al. (2012)

showed that tropospheric heating anomalies over Asia may remotely lead to warming in the United States via changes in the large-scale atmospheric circulation. Wang (2007, 2009) found that direct radiative forcing by BC could impact convective precipitation across the tropics, even far away from the BC sources. In the present study, one of our aims is to consider the remote impacts of anthropogenic aerosol emissions from Asia.

The studies mentioned above have shown that at least four mechanisms should be considered when assessing the climate impacts of Asian aerosols: 1) atmospheric heating by absorbing aerosols, 2) surface cooling by both scattering and absorbing aerosols, 3) indirect effects on clouds, and 4) SST feedbacks. All four mechanisms are represented in the state-of-the-art climate model we use in this study. The aerosol direct effect, semidirect effect, and indirect effects on stratiform clouds (albedo and lifetime effects) are represented. A three-dimensional dynamical ocean is used, allowing SSTs to respond to the aerosol forcing. In contrast, many of the studies mentioned above used prescribed SSTs or thermodynamical slab oceans. Further information about the climate model configuration can be found in section 2b.

In this study, we investigate the transient climate response to two scenarios of future emissions, described in section 2a. The aerosol emissions are modified in Asia only. We investigate the corresponding impacts on surface temperature and precipitation. In addition to looking at the impacts within Asia, where we have modified the emissions, we also consider impacts on relatively remote locations such as Australia and the Sahel region of North Africa.

2. Method

a. Emission scenarios

Two scenarios are considered:

- 1) The representative concentration pathway 4.5 (RCP4.5; van Vuuren et al. 2011; Lamarque et al. 2011) control, a commonly used reference scenario (e.g., Teng et al. 2012; Rotstayn et al. 2012, 2013; Levy et al. 2013), is a “stabilization” scenario that assumes mitigation of greenhouse gas emissions in the presence of climate policy (van Vuuren et al. 2011). Emissions of BC, SO₂, and organic carbon (OC) are projected to decrease (Fig. 1). Such downward emission trends may occur if alternative fuels such as natural gas increasingly replace coal and biofuels or if the widespread adoption of improved technology allows for a substantial reduction in emissions of BC, SO₂, and OC from coal and other fuels. [The RCP4.5 scenario actually assumes an increase in

energy production from coal but with widespread adoption of advanced technology leading to mitigation of greenhouse gas and aerosol emissions (van Vuuren et al. 2011).]

- 2) The A2x experimental scenario in which anthropogenic BC and SO₂ emissions from the domestic, energy, and industry sectors are significantly enhanced in Asia (Figs. 1 and 2a). This represents a scenario in which economic growth and energy demands cause anthropogenic BC and SO₂ emissions to double in Asia. Because of the increasing trend in coal usage (Steckel et al. 2015), such a scenario may occur in the absence of widespread adoption of emission-reduction technology.

Greenhouse gas concentrations and land-use change are prescribed according to the RCP4.5 scenario. For the RCP4.5 simulations, aerosol and aerosol precursor emissions are also specified according to the RCP4.5 scenario. The aerosol and aerosol precursor emissions, which are processed online by a modal aerosol model with three lognormal modes (MAM3; Liu et al. 2012), cover a number of species: SO₂, primary sulfate, BC, OC, dimethyl sulfide (DMS), and gaseous precursors of secondary organic aerosols (SOAG). The MAM3 RCP4.5 emissions assume that 2.5% of the SO₂ is emitted as primary sulfate (Dentener et al. 2006; Liu et al. 2012).

In the year 2000 in China, coal burning is estimated to have been responsible for 92% of SO₂ emissions and 41% of BC emissions but only 23% of OC emissions [derived from Table 1 of Lu et al. (2011)]. If burning of coal were to increase substantially, as assumed in the A2x experimental scenario, this would result in a substantial increase in SO₂ and BC emissions, but the effect on OC emissions would be comparatively smaller. The climatic effects of a change in OC emissions would likely be even smaller compared to the effects of changes in the SO₂ and BC emissions; sulfate is the dominant aerosol species contributing to direct and indirect radiative effects, and BC is the dominant absorbing aerosol species, contributing to atmospheric heating. Hence, OC emissions are not modified in the idealized experimental scenario used in this study.

The experimental scenario, A2x, is based on the RCP4.5 control configuration, with increased SO₂, primary sulfate, and BC emissions over Asia (10°S–50°N, 60°–160°E; Fig. 2a). Asian anthropogenic SO₂, primary sulfate, and BC emissions from the domestic, energy, and industry sectors are linearly ramped from their year-2010 values in 2010 to twice their year-2000 values in 2030. These three sectors are the ones that might be most clearly impacted by a shift to burning more coal. In

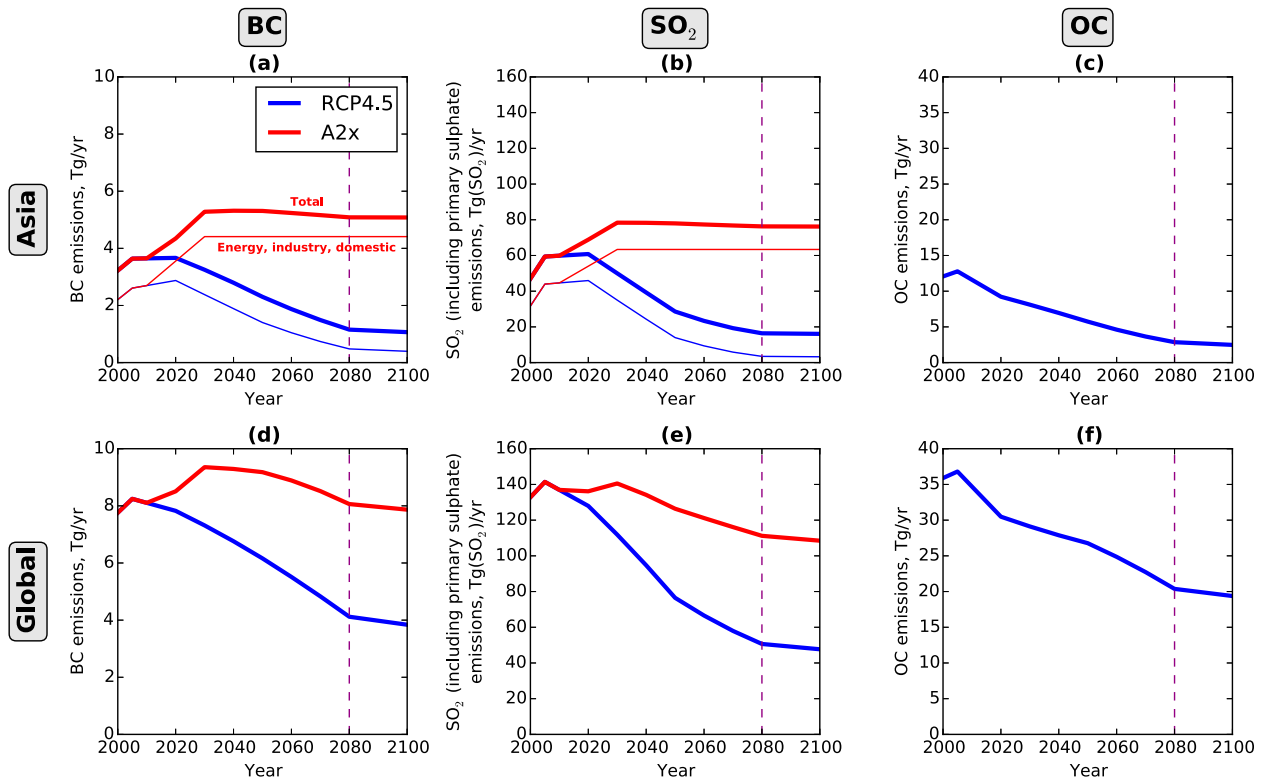


FIG. 1. Time series of annual emission of (a),(d) BC, (b),(e) SO₂ (including primary sulfate), and (c),(f) OC for the two transient scenarios (RCP4.5 and A2x) summed across two different regions: (a)–(c) Asia (see Fig. 2a) and (d)–(f) global. The thicker lines show the total emissions, while the thinner lines in (a),(b) show the subset of emissions that have been edited (anthropogenic energy, industry, and domestic sectors) in Asia. The purple dashed line indicates the year-2080 emissions used in the prescribed-SST simulations (pRCP4.5 and pA2x). Continuous volcanic sulfur emissions of approximately 25 Tg yr⁻¹ of SO₂ contribute to the total global SO₂ emissions; 2.5% of the SO₂ is emitted as primary sulfate. The A2x OC emissions are identical to the RCP4.5 OC emissions.

Asia, these three sectors are responsible for 68% of the BC and 67% of the year-2000 SO₂ emissions. Emissions from the transportation, shipment, waste treatment, and agricultural waste burning sectors are not modified, and they follow the RCP4.5 scenario. After 2030, the SO₂, primary sulfate, and BC emissions from the domestic, energy, and industry sectors remain constant at twice their year-2000 values. Year-2000 values have been chosen as the reference for the doubling. However, the ramping starts in 2010, not 2000, because the transient simulations are initialized mid-decade, in 2006. In addition to modifying the emitted mass concentrations, the corresponding emitted number concentrations of primary sulfate and BC are also modified using the same scaling rules, maintaining the same size distributions.

To clarify, these modifications to the A2x emissions are idealized. In reality, future SO₂ and BC emissions will likely follow different evolution pathways in different parts of Asia (see, e.g., Fiore et al. 2012).

Figure 1a shows the BC emissions from Asia for the two different scenarios. The thinner lines show the

emissions from the domestic, energy, and industry sectors only, illustrating the modifications to the emissions. The linear ramping for the A2x scenario can be seen. The thicker lines show the total BC emissions, including BC from other sources that have not been modified. At the beginning of the twenty-first century, BC emissions from the domestic, energy, and industry sectors dominate. However, for RCP4.5 it can be seen that emissions from these sectors are projected to decrease to much lower values at the end of the twenty-first century.

Figure 1d shows the global BC emissions. For RCP4.5, the global BC emissions decrease substantially over the century. The modifications in Asia for A2x have a large impact on the global emissions. The A2x BC emissions increase before 2030 due to the ramped increase in Asia. After 2030, the A2x emissions have a shallow decreasing trend due to reductions outside Asia.

It is worth noting that the estimate of present-day BC emissions used in RCP4.5 (approximately 8 Tg yr⁻¹ globally) is significantly lower than a more recent top-down estimate of 17.8 ± 5.6 Tg yr⁻¹ (Cohen and Wang

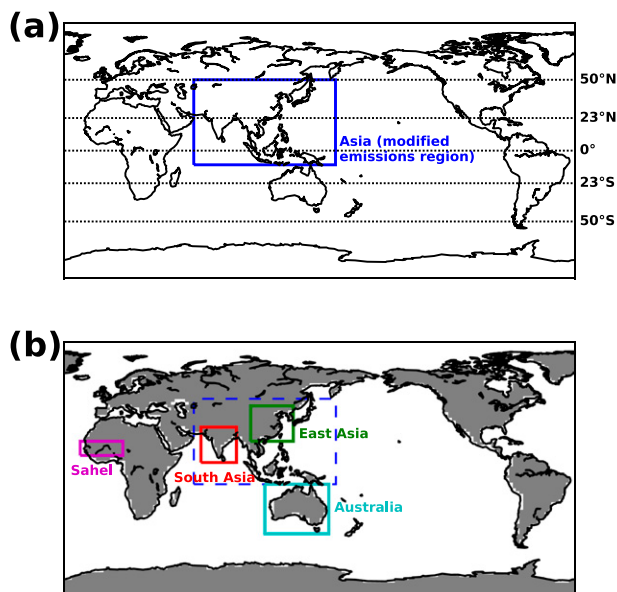


FIG. 2. Maps showing regions referred to in this paper. (a) The Asian region (10°S – 50°N , 60° – 160°E) over which SO_2 (including primary sulfate) and BC emissions have been modified. (b) Four regions for which time series are presented in section 3: East Asia (20° – 45°N , 100° – 130°E), South Asia (5° – 30°N , 65° – 90°E), Australia (10° – 45°S , 110° – 155°E), and the Sahel (10° – 20°N , 20°W – 10°E). The dashed blue rectangle is the Asian region shown in (a). The gray shading indicates grid boxes where the land fraction is greater than 0.9, the threshold used for land-only masking.

2014). Hence the BC emissions may be underestimated in this study, even in the A2x scenario.

The temporal pattern of the SO_2 emissions (Figs. 1b,e) is generally similar to that of the BC emissions. One exception is that for A2x the global SO_2 emissions are relatively flat before 2030, showing that the increased SO_2 emissions in Asia are largely offset by reductions in other parts of the world.

The OC emissions (Figs. 1c,f), which are not modified, represent another source of anthropogenic aerosol. In Asia, there is a decreasing trend, with a reduction of approximately 80% over the course of the century. A decreasing trend is also found globally.

b. Model configuration

1) TRANSIENT MINI-ENSEMBLE

A fully coupled atmosphere–ocean configuration of the Community Earth System Model (CESM), version 1.0.4, is used in this study. The three-dimensional dynamical ocean, land, and sea ice components are similar to those used in the Community Climate System Model, version 4 (CCSM4; Gent et al. 2011). However, the Community Atmosphere Model, version 5 (CAM5; Neale et al. 2012), rather than CAM4, is used here. This

configuration of CESM is referred to as CESM1 (CAM5) (Meehl et al. 2013). CAM5 contains a modal aerosol model with three lognormal modes (MAM3) (Liu et al. 2012). MAM3 includes sulfate, primary organic carbon, secondary organic aerosol, black carbon, sea salt, and soil dust. Although biases remain, MAM3 “is able to qualitatively capture the observed geographical and temporal variations of aerosol mass and number concentrations, size distributions, and aerosol optical properties” (Liu et al. 2012, p. 709). The aerosols have been coupled to the stratiform cloud microphysics, allowing aerosol indirect effects to be represented (Morrison and Gettelman 2008; Gettelman et al. 2010). Compared to many other general circulation models, CAM5 is known to produce weak net aerosol direct radiative forcing but a relatively strong negative total radiative flux perturbation (Table 7 of Shindell et al. 2013) due to aerosol indirect effects (Ghan et al. 2012).

Two earlier studies have used CAM5 to investigate the effects of aerosols on climate in Asia; Ganguly et al. (2012) used CAM5 with a slab ocean to investigate the equilibrium response of the South Asian monsoon to anthropogenic aerosols, and Jiang et al. (2013) used CAM5 with prescribed SSTs to investigate how East Asian clouds and precipitation respond to different aerosol types. In addition, an earlier study by Liu et al. (2011) also investigated how aerosols affect East Asian clouds and precipitation, using CAM3.5. The methodology of the present study differs from these earlier studies in two important ways: first, a three-dimensional dynamical ocean is used, and second, the transient climate response to scenarios of future emissions is investigated.

In this study, the atmosphere model is run on a finite volume grid with a horizontal resolution of $1.9^{\circ} \times 2.5^{\circ}$ and 30 levels. The land model is run on the same horizontal grid. The ocean and sea ice models are run on a displaced pole grid with a horizontal resolution of approximately $1^{\circ} \times 1^{\circ}$.

For each emission scenario (RCP4.5 and A2x), to account for model internal variability, an ensemble of three transient simulations is produced. The simulations are initialized using three different sets of year-2006 initial conditions from a three-member ensemble of historical twentieth-century simulations. They finish at the end of 2099.

2) PRESCRIBED-SST SIMULATIONS

To aid interpretation of the transient ensemble results, two additional simulations are also performed using prescribed sea surface temperatures (SSTs) at their year-2000 climatological values. Year-2000 greenhouse gas concentrations are also prescribed. The two

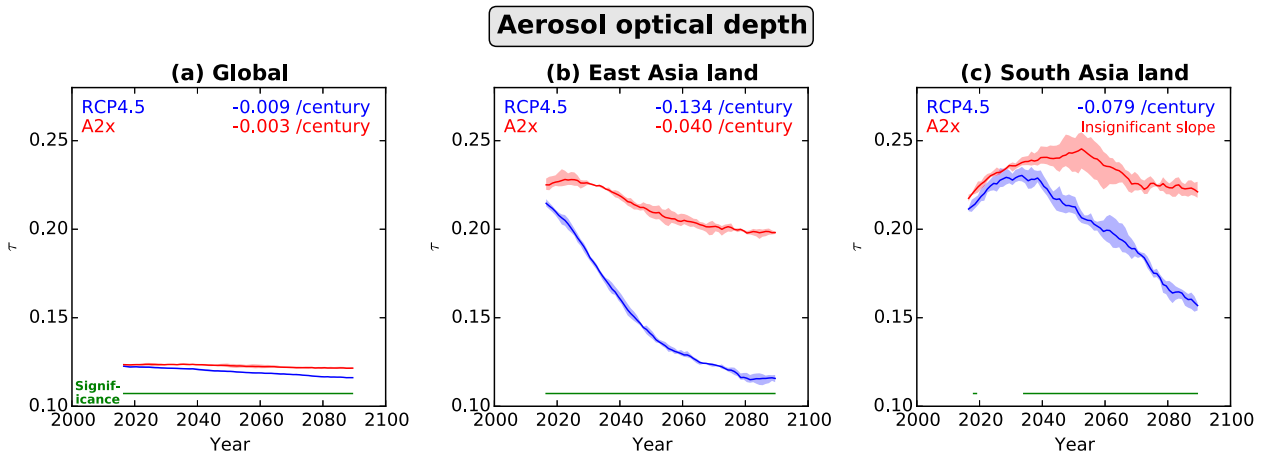


FIG. 3. Time series of total (anthropogenic plus natural) τ in the visible band for the transient ensembles (RCP4.5 and A2x) averaged across three different regions: (a) global (land and ocean), (b) East Asia land only, and (c) South Asia land only (land fraction >0.9 ; Fig. 2b). The blue and red lines show ensemble mean 20-yr moving means. The shaded area envelopes the range within the ensembles, according to 20-yr means for each individual ensemble member. The green lines indicate statistically significant differences, tested using an independent two-sample t test with a two-tailed p -value threshold of 0.05 (see appendix). Linear regression slopes, fitted to the ensemble-mean annual mean data, are written near the top of each panel. Insignificant slope indicates cases where the linear regression slope is statistically insignificant at a two-tailed p -value threshold of 0.05 (see appendix).

prescribed-SST simulations differ only in their aerosol emissions:

- (i) Year-2080 aerosol emissions for the RCP4.5 scenario (pRCP4.5).
- (ii) Year-2080 aerosol emissions for the A2x scenario (pA2x).

The prescribed-SST simulations are each run for 15 years. The first 2 years and 11 months are treated as spinup. The remaining 12 years (starting in December of the third year) are used in the analysis.

A radiative flux perturbation (RFP) approach (Haywood et al. 2009) is used to quantify the radiative effects of the aerosol emission modifications. The top-of-atmosphere RFP differences are decomposed using the method recommended by Ghan (2013). To accomplish this, the radiation scheme is called twice: the first call (interactive) includes all aerosol species, and the second call (diagnostic) excludes all aerosol species from the radiation calculation, allowing diagnosis of “clean sky” fluxes. In addition to allowing diagnosis of RFPs, the prescribed-SST simulations facilitate consideration of the “fast response” (Bala et al. 2010) to the aerosol forcing.

3. Results and discussion

a. Aerosol optical depth

In the RCP4.5 ensemble, global mean aerosol optical depth τ decreases at a rate of -0.009 century $^{-1}$ over the

course of the twenty-first century (Fig. 3a). The A2x global mean τ decreases at a slower rate of -0.003 century $^{-1}$. These decreasing τ trends are consistent with the decreasing global emissions trends of BC, SO₂, and OC (Figs. 1d–f).

Over East Asia, RCP4.5 τ decreases rapidly until 2060, before slowing toward the end of the century (Fig. 3b). This trend approximately mirrors the trends in the Asian BC and SO₂ emissions (Figs. 1a,b). Unlike the modified Asian BC and SO₂ emissions, the A2x τ decreases slowly over East Asia, even near the start of the century. This shows that the increase in Asian SO₂ and BC emissions is not large enough to dominate over a decreasing τ trend over East Asia, although the increased emission of these species do offset the decreasing τ trend to a large extent. The decreasing τ trend over East Asia is likely due to a decreasing OC emission trend locally, particularly steep between 2020 and 2050 (Fig. S1a in the supplemental material), although decreasing emissions of BC and SO₂ outside Asia might also play a role.

Over South Asia, RCP4.5 τ only starts decreasing after approximately 2030 (Fig. 3c). This is due to increasing aerosol emissions over South Asia at the start of the century in RCP4.5 (e.g., Fig. S1b in the supplemental material). The A2x τ increases at the start of the century before slowly decreasing later in the century. The increasing trend at the start is consistent with the increasing SO₂, BC, and OC emissions, while the later decrease is consistent with the later reduction in OC emissions (Fig. S1b).

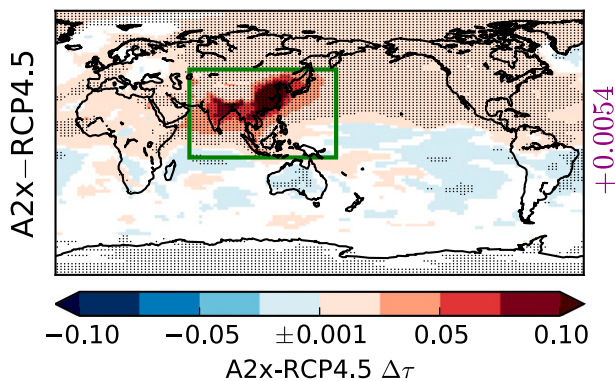


FIG. 4. Map of annual-mean total τ A2x – RCP4.5 differences for the transient ensembles averaged across 2080–99. Ensemble mean differences are shown. White indicates mean differences smaller than ± 0.001 . Stippling indicates statistically significant differences, tested using an independent two-sample t test with a two-tailed p -value threshold of 0.05 (see appendix). The area-weighted mean difference is provided at the right side of the map. The green rectangle indicates the Asian region over which emissions have been modified.

When averaged across 2080–99, A2x τ is larger than RCP4.5 τ across most of the Northern Hemisphere (Fig. 4). Over parts of Asia, where the emissions have been modified, differences as large as 0.10 are found. Over parts of the tropical and subtropical ocean in the Southern Hemisphere, A2x τ is lower than RCP4.5 τ , likely due to differences in 10-m wind speed (Fig. S8 in the supplemental material) affecting emission of sea-salt aerosol. The τ differences over Antarctica are very small (less than 0.001).

b. Radiative flux perturbations

Earlier studies have investigated CESM1(CAM5) RFPs for present-day (PD) aerosol emissions relative to year-1850 emissions (Ghan et al. 2012) and for future RCP4.5 year-2100 emissions relative to PD emissions (Meehl et al. 2013). Interested readers are referred to these two papers for details. It is worth noting that RCP4.5 simulations project a weakening of the radiative effect of aerosols, in both CESM1(CAM5) (Meehl et al. 2013) and other climate models (Rotstayn et al. 2013), as aerosol emissions decline, leading to a positive year-2100 – PD radiative effect.

In this paper, the top-of-atmosphere RFP differences are calculated with respect to pRCP4.5, which uses year-2080 aerosol emissions from the RCP4.5 scenario, rather than a simulation using year-1850 emissions. The increased aerosol emissions in pA2x, which uses year-2080 aerosol emissions from the A2x scenario, lead to an additional global mean negative shortwave (SW) RFP of -0.88 W m^{-2} (Fig. 5). The signal is strongest in parts of Asia, where the aerosol emissions have been

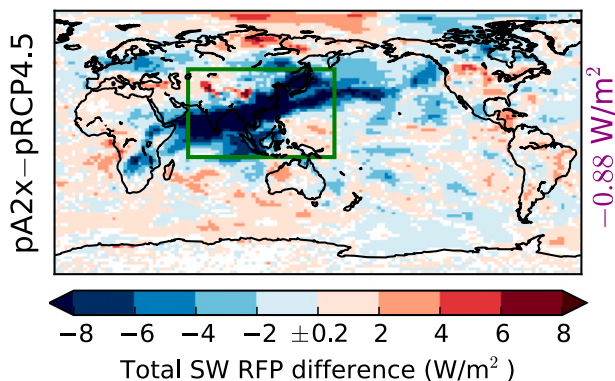


FIG. 5. Map of total SW top-of-atmosphere RFP pA2x – pRCP4.5 differences for the prescribed-SST simulations with year-2080 aerosol emissions. The averaging period is 12 years. Because of the small sample size of 12 annual means, significance is not tested. White indicates differences smaller than $\pm 0.2 \text{ W m}^{-2}$. The area-weighted mean difference is provided at the right side of the map. The green rectangle indicates the Asian region over which emissions have been modified.

modified, with differences larger than 8 W m^{-2} at some locations.

Using the procedure recommended by Ghan (2013), the SW RFP differences are decomposed into direct radiative effect (DRE; Fig. S2 in the supplemental material), clean-sky cloud radiative effect (Fig. S3 in the supplemental material), and surface albedo effect (Fig. S4 in the supplemental material). The aerosol DRE component is small and opposite in sign (Fig. S2) compared to the total SW RFP (Fig. 5). The positive black carbon DRE is larger than the negative sulfate DRE. Ghan et al. (2012), who decomposed PD – year-1850 DREs into components for individual species, also found that the positive DRE for BC more than offsets the negative DRE for sulfate.

By far the largest component contributing to the total SW RFP differences (Fig. 5) is associated with changes in cloud forcing (Fig. S3). The global mean pA2x – pRCP4.5 difference in cloud SW RFP is -0.97 W m^{-2} . This difference is primarily due to the aerosol indirect effect on clouds. Ghan et al. (2012) found the PD – year-1850 semidirect component to be statistically insignificant.

The cloud SW RFP is partially offset by the longwave (LW) RFP, which is generally opposite in sign (Fig. 6). The global mean pA2x – pRCP4.5 difference in cloud LW RFP is $+0.49 \text{ W m}^{-2}$. Interestingly, negative pA2x – pRCP4.5 differences in cloud LW RFP larger than -2 W m^{-2} are found over the Sahel region of North Africa. The relatively large LW RFP differences, which generally correspond to differences in high cloud cover (Fig. S5 in the supplemental material), are likely due to

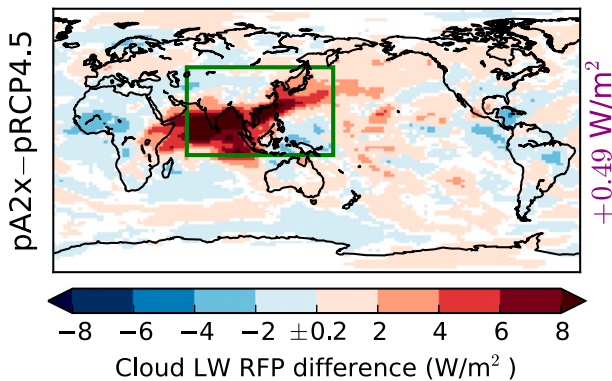


FIG. 6. As in Fig. 5, but for clean-sky cloud LW top-of-atmosphere RFP pA2x – pRCP4.5 differences.

ice nucleation affecting cirrus cloud formation and radiative properties (Ghan et al. 2012; Gettelman et al. 2012).

These results indicate that, even with prescribed SSTs, aerosol emissions from Asia can have remote radiative impacts elsewhere.

c. Surface temperature: A global overview

For the transient ensembles, averaged across 2080–99, the enhanced Asian aerosol emissions in A2x lead to a widespread cooling, relative to RCP4.5, across most of the Northern Hemisphere (Fig. 7). Relative cooling is also found over most of Africa, Australia, and South America. The cloud SW RFP (Fig. S3) is predominantly responsible for the widespread cooling. Differences larger than 1.0°C are found over parts of the Arctic polar regions. This large relative cooling in the Arctic is associated with differences in sea ice fractional cover (Fig. S9 in the supplemental material), suggesting that surface temperature and sea ice fraction are coupled via a surface albedo feedback. The surface albedo feedback, in addition to a potentially stronger temperature feedback, is known to amplify the temperature change signal in the Arctic (Pithan and Mauritsen 2014).

The cooling is relative between these transient ensembles rather than absolute because both ensembles experience greenhouse gas-induced warming over the twenty-first century. Over the Northern Hemisphere, RCP4.5 warms at a rate of 2.9°C century⁻¹, while A2x warms at a slower rate of 2.4°C century⁻¹ (Fig. 8a). Over the Southern Hemisphere, the enhanced aerosol emissions in A2x have little impact on the hemispheric mean surface temperature, and both RCP4.5 and A2x warm at a rate of 2.0°C century⁻¹ (Fig. 8b). The stronger aerosol-induced cooling of the Northern Hemisphere compared to the Southern Hemisphere impacts the

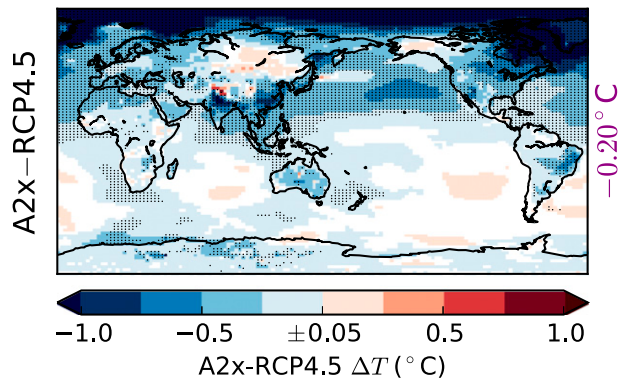


FIG. 7. Map of annual-mean surface temperature A2x – RCP4.5 differences for the transient ensembles averaged across 2080–99. Ensemble mean differences are shown. White indicates mean differences smaller than $\pm 0.05^{\circ}\text{C}$. Stippling indicates statistically significant differences, tested using an independent two-sample t -test with a two-tailed p value threshold of 0.05 (see appendix). The area-weighted mean difference is provided at the right side of the map.

interhemispheric temperature gradient (Fig. 9; Table S1 in the supplemental material).

d. Precipitation: A global overview

In RCP4.5, both the Northern Hemisphere tropics and the Southern Hemisphere tropics experience increasing precipitation trends (Figs. 10a,b), as would be expected in a global warming scenario. Held and Soden (2006) found a global mean precipitation sensitivity of approximately 2% °C⁻¹ when they analyzed results from a number of models.

Although greenhouse gas-induced warming may be the primary driver of global mean precipitation increases, aerosol forcing likely dominates changes in the large-scale distribution of precipitation via surface temperature gradients (Wang 2015). In the ensembles analyzed here, the aerosol-induced modification to the interhemispheric temperature gradient (Fig. 9) does indeed impact the zonal-mean precipitation rate R distribution (Fig. 11). The enhanced aerosol emissions in A2x strongly suppress the Northern Hemisphere tropical precipitation trend while simultaneously enhancing the Southern Hemisphere tropical precipitation trend (Figs. 10a,b). The strong aerosol-induced suppression in the Northern Hemisphere tropics leads to a southward shift of the intertropical convergence zone (ITCZ), an effect that is especially evident between 60°–160°E (Fig. 11b). These results are consistent with other studies that have found that the position of the ITCZ is sensitive to changes in the interhemispheric temperature gradient [e.g., Wang 2004; for a review, see Chiang and Friedman (2012)].

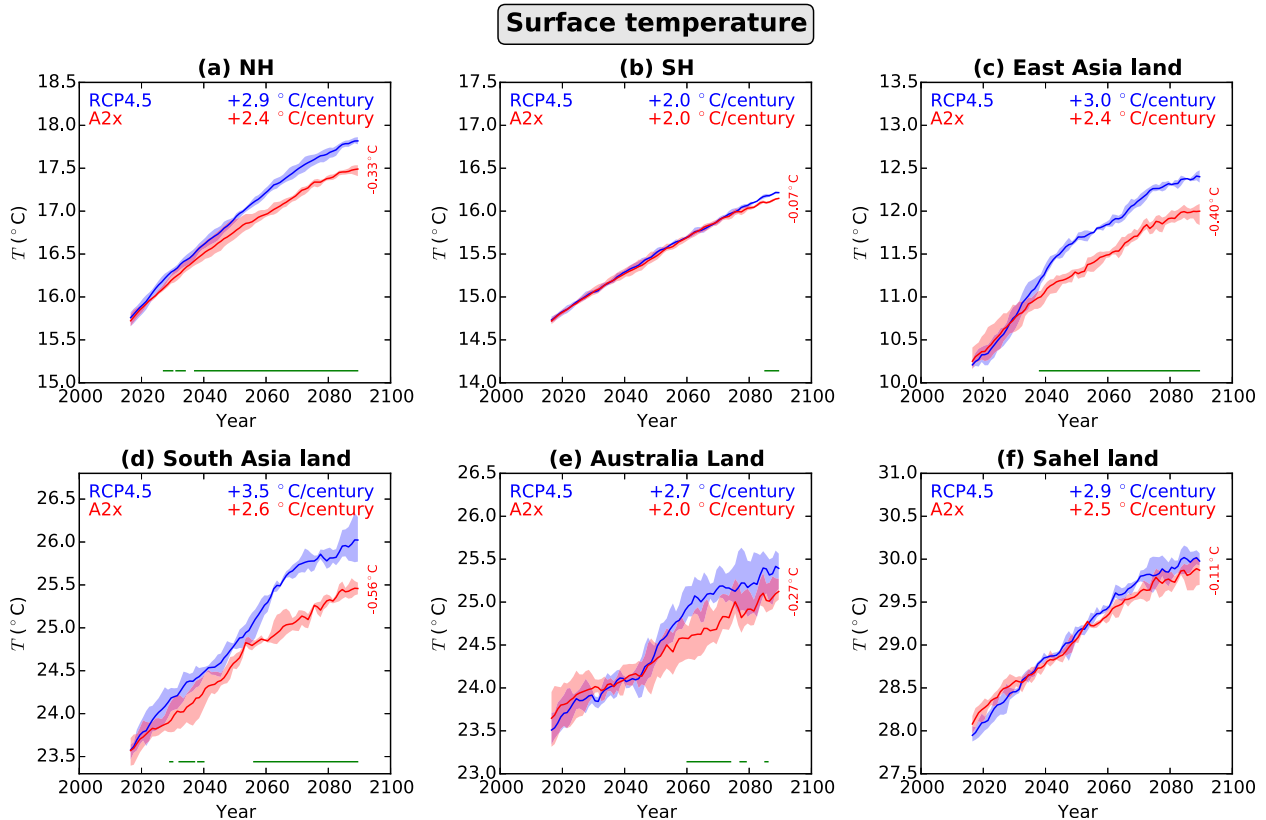


FIG. 8. Time series of surface temperature for the transient ensembles (RCP4.5 and A2x), averaged across six different regions: (a) Northern Hemisphere (land and ocean), (b) Southern Hemisphere (land and ocean), (c) East Asia land only, (d) South Asia land only, (e) Australia land only, and (f) Sahel land only (land fraction >0.9 ; Fig. 2b). The blue and red lines show ensemble-mean 20-yr moving means. The A2x – RCP4.5 differences for the final 20-yr period (2080–99) are given in vertical red text at the right in each panel. The shaded area envelopes the range within the ensembles, according to 20-yr means for each individual ensemble member. The green lines indicate statistically significant differences, tested using an independent two-sample t test with a two-tailed p -value threshold of 0.05 (see appendix). Linear regression slopes, fitted to the ensemble-mean annual mean data, are written near the top of each panel. None of slopes are found to be statistically insignificant (see appendix).

Figure 12 shows the regional distribution of precipitation differences, averaged across 2080–99. A mixture of positive and negative A2x – RCP4.5 differences are found. For example, A2x produces less precipitation than RCP4.5 over parts of East Asia, South Asia, North Africa, and Greenland; A2x produces more precipitation than RCP4.5 over Australia and parts of South America. Four of these regions are considered in more detail below.

e. East Asia

Over East Asia, RCP4.5 produces a higher rate of warming during the first few decades, as aerosol emissions decrease, than it does toward the end of the century (Fig. 8c). The average warming rate is $3.0^{\circ}\text{C century}^{-1}$. Because of the aerosol-induced cooling, A2x produces a lower warming trend of $2.4^{\circ}\text{C century}^{-1}$, delaying warming by over two decades toward the end of the century.

Annual precipitation increases at a rate of $27\% \text{ century}^{-1}$ in the RCP4.5 ensemble (Fig. 10c). For A2x, precipitation increases less than half as fast, at a rate of $12\% \text{ century}^{-1}$. This demonstrates that the precipitation increase can be delayed to an even greater extent than the surface temperature increase. The aerosol-induced suppression of precipitation occurs throughout the year, especially during the summer monsoon months between May and August (Figs. 13a,b). Interestingly, in July the southern part of the East Asia region undergoes a precipitation enhancement, although this is statistically insignificant [see also Gu et al. (2006)]. This southern enhancement could be interpreted either as an extension of the heavy precipitation in June or as a southward shift of the precipitation pattern for July.

The precipitation rate (Fig. 13a) is well correlated with vertical velocity at 500 hPa (ω_{500} ; Fig. 14a), a measure of midtropospheric vertical velocity. Similarly, A2x – RCP4.5 ΔR (Fig. 13b) is generally well correlated

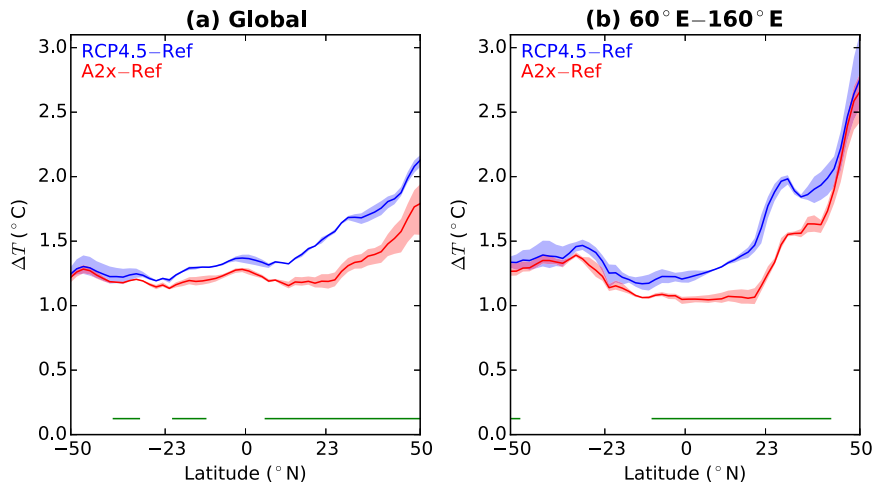


FIG. 9. Zonal-mean annual-mean surface temperature differences, relative to the RCP4.5 ensemble mean averaged across 2010–29 (Ref), for the transient ensembles (RCP4.5 and A2x) averaged across 2080–99. Two different longitude bounds are shown: (a) global and (b) 60°–160°E (corresponding to the longitude bounds of the Asia region over which emissions have been modified). Both land and ocean data are used. The blue and red lines show the ensemble means. The shaded area envelopes the range within the ensembles, according to the 2080–99 mean for each individual ensemble member. The green lines indicate statistically significant differences between the ensembles, tested using an independent two-sample t test with a two-tailed p -value threshold of 0.05 (see appendix).

with $\Delta\omega_{500}$ (Fig. 14b). Suppression of rainfall is associated with anomalous downward motion in the mid-troposphere (generally indicating suppressed ascent; cf. Figs. 14b,a). Anomalous upward motion (indicating suppressed subsidence) occurs over northern East Asia during January, February, and May. Farther south, near 5°–10°N, anomalous downward motion occurs throughout the year. These features suggest that the enhanced aerosols in A2x weaken the East Asian branch of the Hadley circulation.

As discussed in the introduction, several previous studies have considered the impact of anthropogenic aerosols on the East Asian monsoon. Based on these studies, a general suppression of the East Asian summer monsoon precipitation may arise because of atmospheric heating by BC and associated circulation changes (Menon et al. 2002; Lau et al. 2006). Precipitation in north China may be further suppressed by surface cooling (Jiang et al. 2013).

Although the “slow response” due to SST cooling may play a role, our results suggest that it is not an essential component of the East Asian precipitation suppression mechanism; the fast response (Bala et al. 2010) also exhibits suppression of precipitation over East Asia (Fig. S7 in the supplemental material).

f. South Asia

Over South Asia, the RCP4.5 ensemble warms at a rate of 3.5°C century⁻¹ (Fig. 8d). The A2x ensemble warms at a

slower rate of 2.6°C century⁻¹, showing that the aerosol cooling effect is larger than the BC warming effect.

There are no obvious annual precipitation trends over South Asia (Fig. 10d). Warming may not have a large impact on annual precipitation over this region. However, the enhanced aerosol emissions in A2x appear to lead to a suppression of precipitation. When averaged across 2080–99, A2x produces 3.5% less precipitation than RCP4.5, although this difference is not statistically significant.

Over southern India, the aerosol-induced suppression of annual precipitation is particularly pronounced and statistically significant (Fig. 12). Such a suppression is not found in the corresponding fast response prescribed-SST simulations (Fig. S7), suggesting that the SST slow response is an important component of the mechanism by which the South Asian monsoon is suppressed. The enhanced aerosol emissions in A2x lead to a relative cooling of the SSTs in the Bay of Bengal and the Arabian Sea. As pointed out by Ramanathan et al. (2005) and Meehl et al. (2008), such cooling of the SSTs can lead to weakened SST gradients and hence a suppression of monsoon precipitation.

The suppression of precipitation is generally strongest during the summer monsoon season (Figs. 13c,d). This suppression of the summer monsoon precipitation corresponds to a weakening of the Hadley circulation during the summer months (Figs. 14c,d).

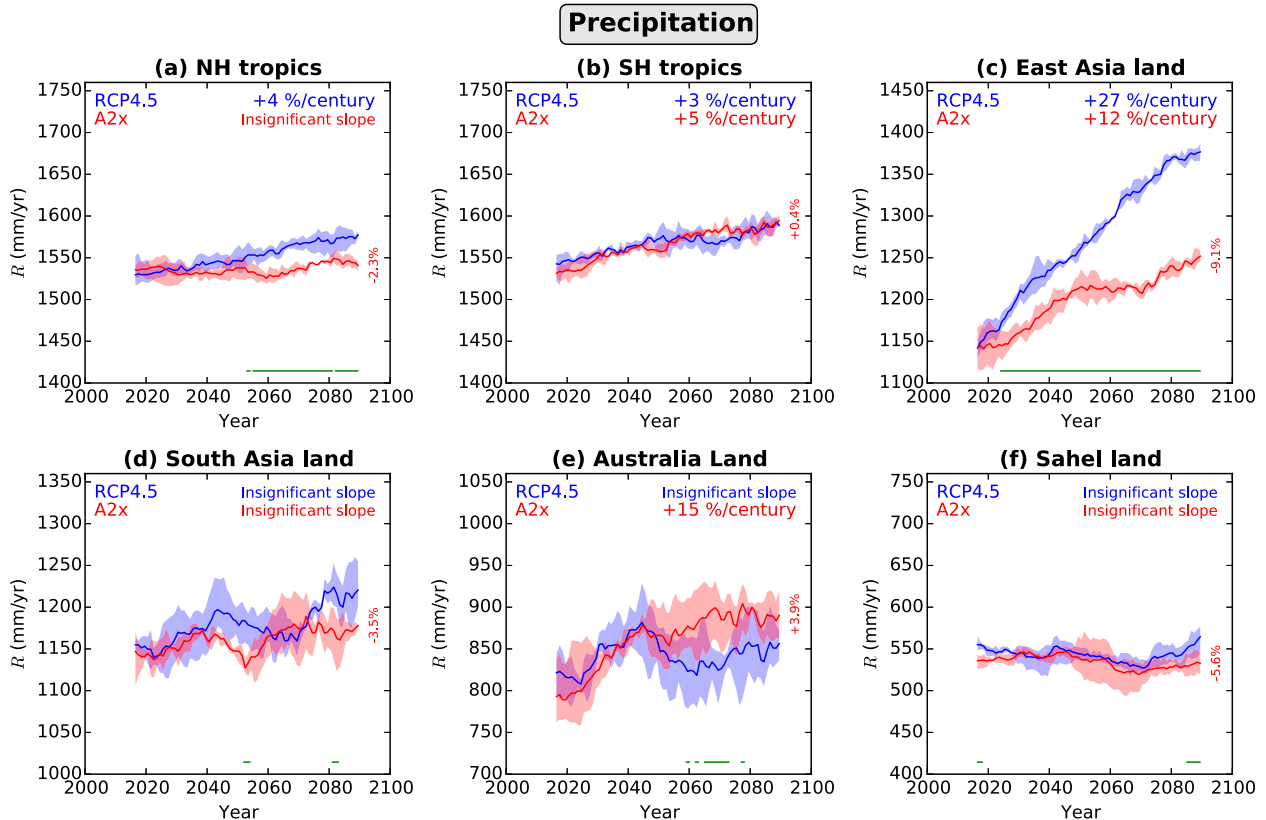


FIG. 10. Time series of annual precipitation rate R for the transient ensembles (RCP4.5 and A2x) averaged across six different regions: (a) Northern Hemisphere tropics (0° – 23° N, land and ocean), (b) Southern Hemisphere tropics (0° – 23° S, land and ocean), (c) East Asia land only, (d) South Asia land only, (e) Australia land only, and (f) Sahel land only (land fraction >0.09 ; Fig. 2b). The blue and red lines show ensemble-mean 20-yr moving means. The A2x – RCP4.5 differences for the final 20-yr period (2080–99) are given in vertical red text at the right in each panel. The shaded area envelopes the range within the ensembles, according to 20-yr means for each individual ensemble member. The green lines indicate statistically significant differences, tested using an independent two-sample t test with a two-tailed p -value threshold of 0.05 (see appendix). Linear regression slopes ($\%$ century $^{-1}$, relative to the regression line intercept at year 2007), fitted to the ensemble-mean annual mean data, are written near the top of each panel. Insignificant slope indicates cases where the linear regression slope is statistically insignificant at a two-tailed p -value threshold of 0.05 (see appendix).

Strong suppression of precipitation also occurs in January over southern South Asia (Fig. 13d), a feature that indicates an earlier arrival of the dry season (Fig. 13c). The suppression of R in January over southern South Asia, and farther south during February and March, is accompanied by anomalous downward motion in the midtroposphere (Fig. 14d). This anomalous downward motion during January–March indicates a southern extension of the large-scale subsidence over South Asia during these months (Fig. 14c). This is consistent with a southward shift of the Hadley circulation and ITCZ near South Asia during January–March.

In contrast to the general suppression of precipitation over southern and central South Asia, the enhanced aerosol emissions in A2x appear to enhance precipitation during May and June in northern South Asia, although this enhancement is statistically insignificant (Fig. 13d). This is accompanied by an anomalous upward

motion in the midtroposphere (corresponding to enhanced ascent; Figs. 14c,d). These results suggest an earlier arrival of monsoon precipitation in northern South Asia, a feature that is consistent with the elevated heat pump hypothesis of Lau et al. (2006) and the moist static energy perspective of Wang et al. (2009) and Lee et al. (2013).

g. Australia

The Asian aerosol emissions can affect other regions outside of Asia. Over Australia, RCP4.5 produces a warming trend of $2.7^{\circ}\text{C century}^{-1}$ (Fig. 8e). A2x produces a slower trend of $2.0^{\circ}\text{C century}^{-1}$. It is possible that aerosol-induced enhancement of precipitation (see below), as well as the associated cloud cover changes, may be partially responsible for the cooling of Australia in A2x.

Upward trends in annual precipitation occur over the first few decades, but the trends appear to be relatively

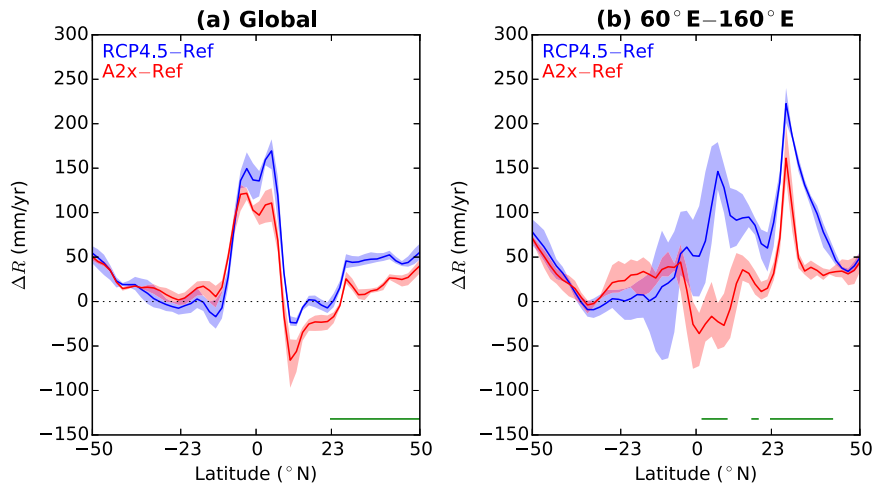


FIG. 11. Zonal-mean annual R differences, relative to the RCP4.5 ensemble mean averaged across 2010–29 (Ref), for the transient ensembles (RCP4.5 and A2x) averaged across 2080–99. Two different longitude bounds are shown: (a) global and (b) 60° – 160° E (corresponding to the longitude bounds of the Asia region over which emissions have been modified). Both land and ocean data are used. The blue and red lines show the ensemble means. The shaded area envelopes the range within the ensembles, according to the 2080–99 mean for each individual ensemble member. The green lines indicate statistically significant differences between the ensembles, tested using an independent two-sample t test with a two-tailed p -value threshold of 0.05 (see appendix).

flat during the second half of the twenty-first century (Fig. 10e). After year 2050, A2x generally produces more precipitation than RCP4.5. When averaged across 2080–99 over Australia, A2x produces 3.9% more precipitation than RCP4.5 does, although this difference is statistically insignificant. However, for some of the earlier periods, including 2060–80, the difference between A2x and RCP4.5 is statistically significant.

Consideration of the seasonal cycle reveals that the largest increases in precipitation occur over northern Australia during March (Fig. 13f). Increases in precipitation occur over central Australia during February–April, although most of these are statistically insignificant. A smaller (and statistically insignificant) suppression of precipitation occurs during November. Comparison of these A2x – RCP4.5 ΔR features with the annual cycle of R (Fig. 13e) reveals two impacts of the enhanced Asian aerosol emissions: first, there is a southward shift of the austral summer monsoon precipitation, consistent with a southward shift of the ITCZ; second, the arrival of the monsoon precipitation may be delayed slightly during November, but the monsoon season lasts longer overall. Rotstayn et al. (2012) have previously noted that large-scale aerosol forcing may enhance December–March precipitation over northwestern Australia via changes in the monsoon flow.

For the prescribed-SST simulations, the enhanced Asian aerosol emissions in pA2x do not appear to consistently enhance annual precipitation over Australia (Fig. S7). This demonstrates that the aerosol-induced

SST slow response and the associated surface temperature gradients play an important role in remotely enhancing the austral summer monsoon over Australia.

h. The Sahel

Over the Sahel region of North Africa, the RCP4.5 ensemble warms at rate of $2.9^{\circ}\text{C century}^{-1}$ (Fig. 8f). The

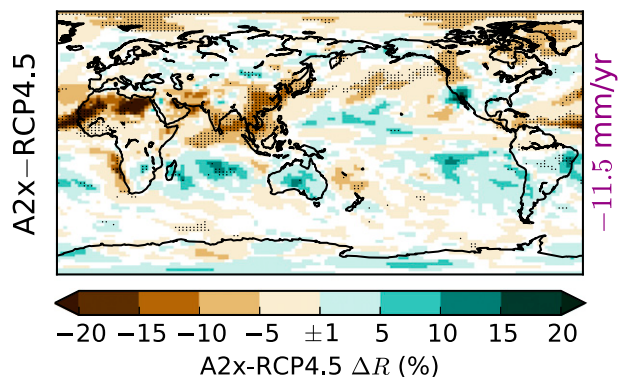


FIG. 12. Map of mean annual R percentage differences (A2x – RCP4.5, relative to RCP4.5) for the transient ensembles, for the period 2080–99. The input R data have been averaged across 2080–99 for each ensemble member, prior to calculating ensemble-mean R data. These ensemble-mean R data were then used to calculate the percentage differences. White indicates mean differences smaller than $\pm 1\%$. Stippling indicates statistically significant differences, tested using an independent two-sample t test with a two-tailed p -value threshold of 0.05 (see appendix). The area-weighted mean absolute difference is provided at the right side of the map.

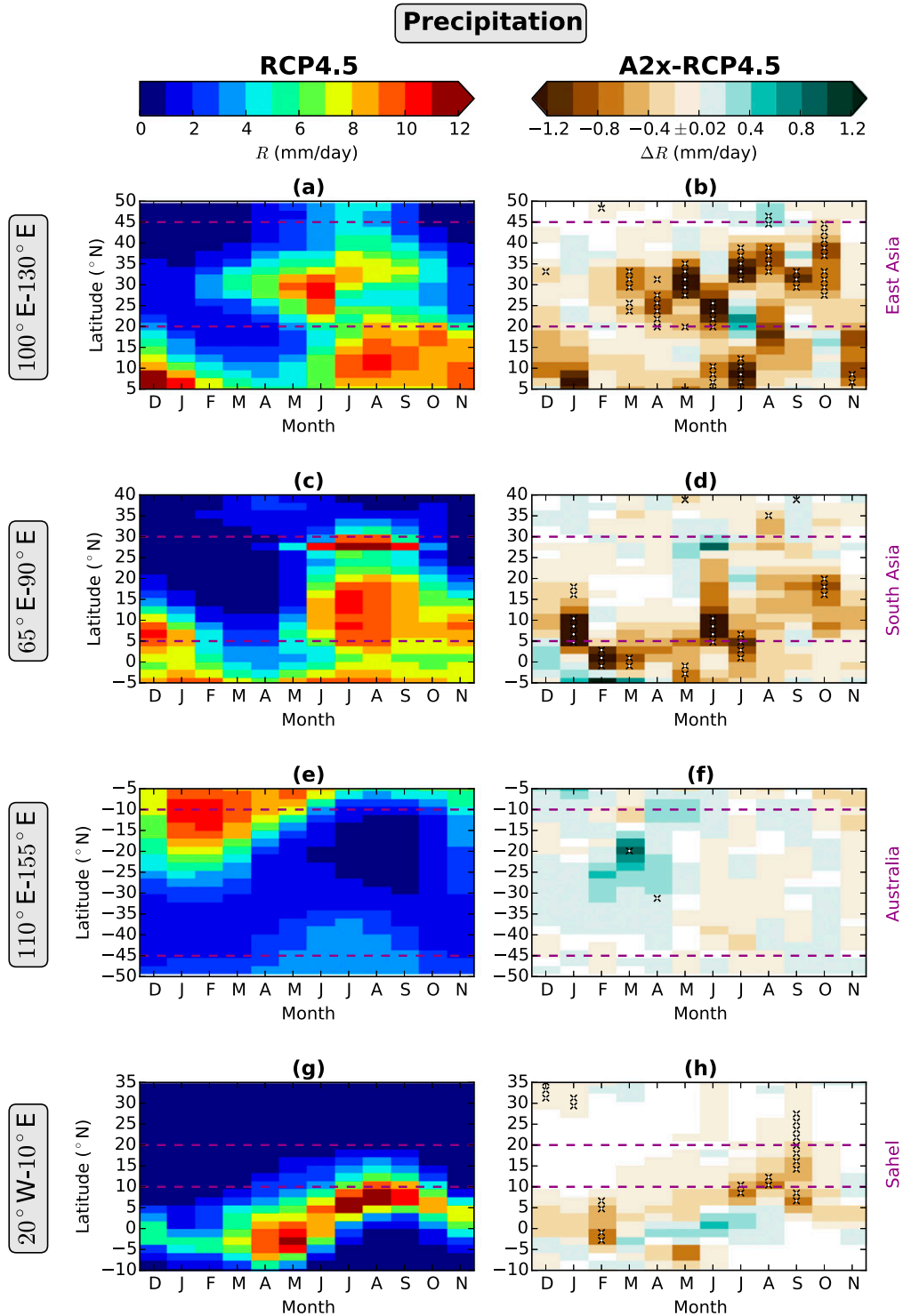


FIG. 13. Hovmöller diagrams of monthly R , showing the seasonal cycle for 2080–99 zonally averaged across different longitude bounds: (a),(b) 100°–130°E (corresponding to the longitude bounds of the East Asia region), (c),(d) 65°–90°E (corresponding to South Asia), (e),(f) 110°–155°E (corresponding to Australia), and (g),(h) 20°W–10°E (corresponding to the Sahel). Shown are (left) the data for the RCP4.5 ensemble, averaged across 2080–99 and all three sets of initial conditions and (right) the A2x – RCP4.5 differences. White indicates differences smaller than ± 0.02 mm day⁻¹. The diagonal crosses indicate statistically significant differences, tested using an independent two-sample t test with a two-tailed p -value threshold of 0.05 (see [appendix](#)). The purple dashed lines indicate the latitude bounds of different regions. Both land and ocean data are used. Note that the y -axis latitude ranges differ between the different rows.

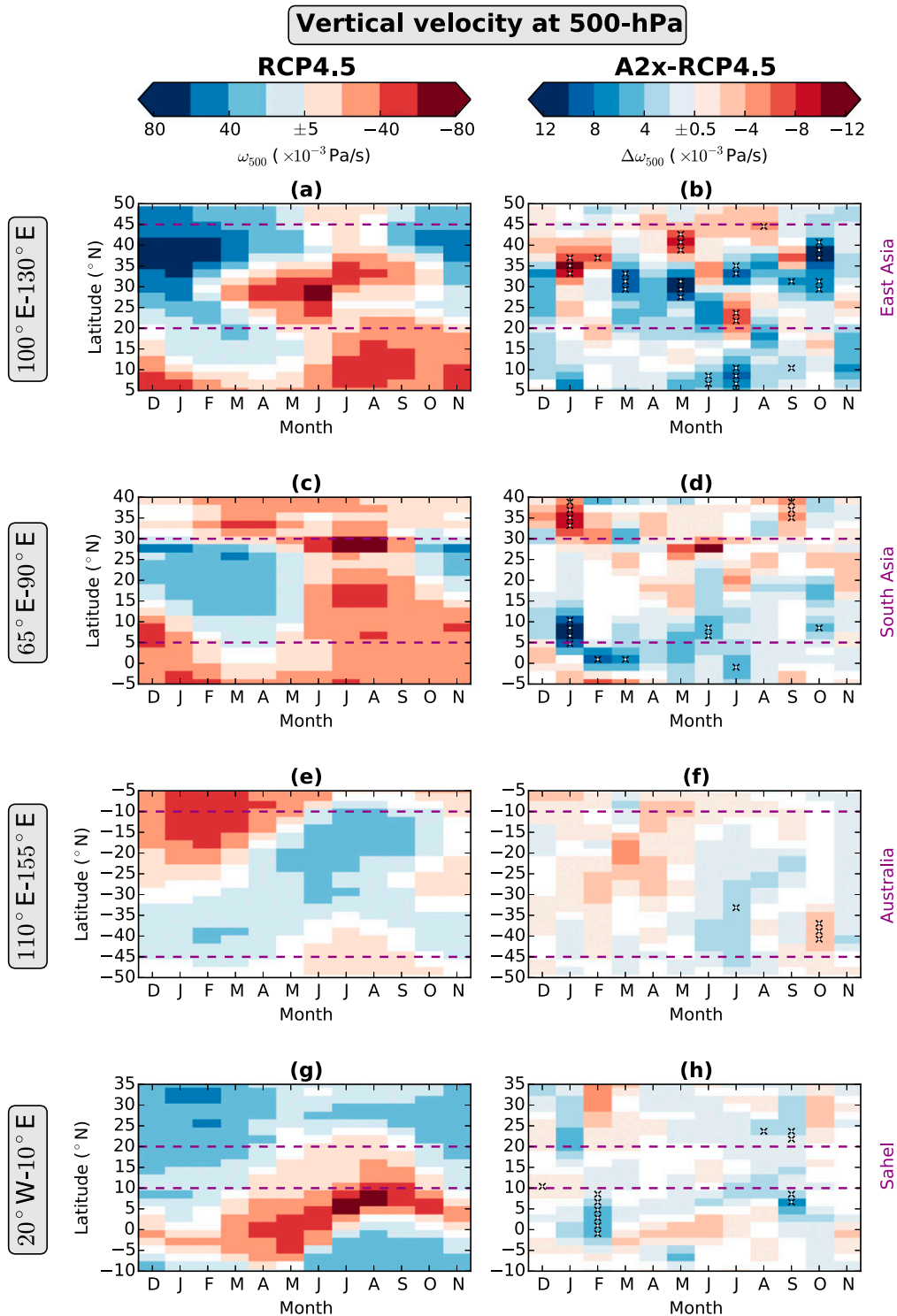


FIG. 14. Hovmöller diagrams of ω_{500} , showing the seasonal cycle for 2080–99 zonally averaged across different longitude bounds: (a),(b) 100°–130°E (corresponding to the longitude bounds of the East Asia region), (c),(d) 65°–90°E (corresponding to South Asia), (e),(f) 110°–155°E (corresponding to Australia), and (g), (h) 20°W–10°E (corresponding to the Sahel). Shown are (left) the data for the RCP4.5 ensemble, averaged across 2080–99 and all three sets of initial conditions and (right) the A2x – RCP4.5 differences. Positive values of ω_{500} indicate downward motion. White indicates values smaller than $5 \times 10^{-3} \text{ Pa s}^{-1}$ at left or $0.5 \times 10^{-3} \text{ Pa s}^{-1}$ at right. The diagonal crosses indicate statistically significant differences, tested using an independent two-sample t test with a two-tailed p -value threshold of 0.05 (see appendix). The purple dashed lines indicate the latitude bounds of different regions. Both land and ocean data are used. Note that the y-axis latitude ranges differ between the different rows.

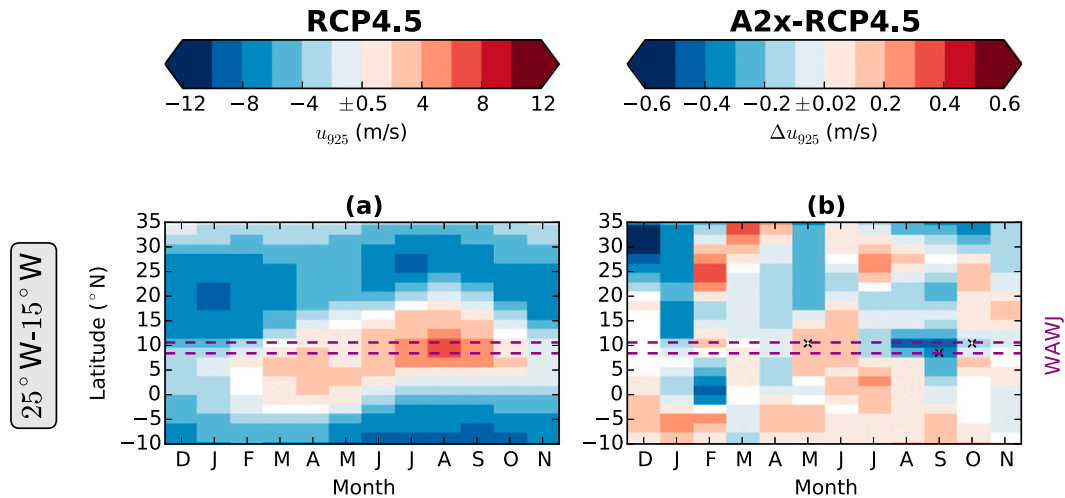


FIG. 15. Hovmöller diagrams of 925-hPa zonal wind u_{925} , showing the seasonal cycle for 2080–99 zonally averaged across 25°–15°W. Shown are (a) the data for the RCP4.5 ensemble averaged across 2080–99 and all three sets of initial conditions and (b) the A2x – RCP4.5 differences. Positive values of u_{925} indicate eastward motion. White indicates values smaller than 0.5 m s^{-1} in (a) or 0.02 m s^{-1} in (b). The diagonal crosses indicate statistically significant differences, tested using an independent two-sample t test with a two-tailed p -value threshold of 0.05 (see appendix). The purple dashed lines indicate the latitude bounds of the region (8.4° – 10.6° N, 25° – 15° W) over which u_{925} is averaged to calculate the strength of the WAWJ (Pu and Cook 2012). Both land and ocean data are used.

A2x ensemble warms at slightly slower rate of $2.5^{\circ}\text{C century}^{-1}$. Negative cloud LW RFP differences (Fig. 6) may contribute toward the cooling of the Sahel in A2x compared to RCP4.5.

Clear annual precipitation trends are not evident (Fig. 10f). However, annual precipitation is generally lower for A2x compared to RCP4.5, especially toward the end of the twenty-first century. When averaged across 2080–99, A2x produces 5.6% less precipitation than RCP4.5 over the Sahel. This suggests that the enhanced Asian aerosol emissions may have a remote climatic effect by suppressing precipitation over the Sahel.

The largest aerosol-induced suppression of precipitation occurs during July–September (JAS; Fig. 13h), consistent with a weakening of the West African monsoon. Sahel precipitation is known to be correlated with the West African westerly jet (WAWJ; Fig. 15a), which transports moisture from the Atlantic Ocean to the Sahel (Pu and Cook 2012). For the transient ensembles analyzed in this paper, approximately half of the variance in Sahel precipitation during JAS can be statistically explained by variance in the WAWJ during JAS (Fig. S10 in the supplemental material). When averaged across 2080–99, the JAS WAWJ is weaker in A2x compared to RCP4.5 (Figs. 15b and 16), suggesting that changes in the WAWJ may indeed be responsible for the A2x – RCP4.5 precipitation difference. However, these results should be treated with caution; although statistically significant A2x – RCP4.5 differences in 925-hPa zonal wind occur over parts of the WAWJ region during

September and October (Fig. 15b), the difference in overall JAS WAWJ strength is statistically insignificant (Fig. 16). The detailed mechanism by which Asian aerosol emissions impact the WAWJ remains unclear, although surface temperature gradients over Africa are likely to play a role.

Previous research has also suggested that the precipitation over the Sahel may be sensitive to interhemispheric temperature gradients (Chiang and Friedman 2012). For example, it has been suggested that the Sahel precipitation might be influenced by North Atlantic Ocean aerosol forcing (Booth et al. 2012) and stratospheric aerosol forcing (Haywood et al. 2013). Recently, using prescribed-SST simulations, Dong et al. (2014) found that emissions of SO_2 from Asia may suppress the West African monsoon, and hence precipitation over the Sahel, via changes in the Walker circulation.

Although the prescribed-SST pA2x – pRCP4.5 fast response can partially explain the suppression of precipitation over the Sahel (Fig. S7), the role of the SST slow response remains unclear. These open questions—namely, the relative importance of the ocean response and the mechanism by which Asian aerosol emissions impact the WAWJ—provide a focus for further research.

4. Conclusions

Using a coupled atmosphere–ocean configuration of CESM1(CAM5), we have investigated the twenty-first century transient climate response to two scenarios of

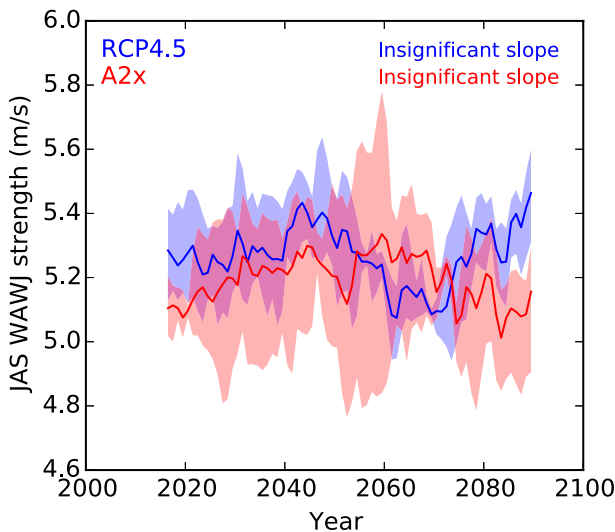


FIG. 16. Time series of strength of WAWJ (925-hPa zonal wind averaged across 8.4°–10.6°N, 25°–15°W; Pu and Cook 2012) during JAS. The blue and red lines show ensemble-mean 20-yr moving means. The shaded area envelopes the range within the ensembles, according to 20-yr means for each individual ensemble member. For each 20-yr period, statistical significance is tested using an independent two-sample t test with a two-tailed p -value threshold of 0.05 (see appendix), but none of the differences are found to be significant. The linear regression slopes are also found to be statistically insignificant (see appendix), as indicated by insignificant slope.

future aerosol emissions. To aid interpretation of the transient mini-ensembles, we have also performed two corresponding prescribed-SST simulations, forced by year-2080 aerosol emissions.

In RCP4.5, the control scenario, anthropogenic aerosol and precursor emissions generally decrease over Asia during the course of the twenty-first century, as would be the case if coal usage were to be phased out in favor of alternative fuels such as natural gas. In A2x, the enhanced Asian emission scenario, Asian emissions of SO₂, primary sulfate, and BC emissions from the domestic, energy, and industry sectors were set to twice their year-2000 values from 2030 onward. A2x can be interpreted as an extreme scenario in which energy demand drives a rapid increase in emission from coal and other fuels.

We have found that the radiative impacts of the Asian anthropogenic aerosols extend across much of the world, particularly the Northern Hemisphere. Cloud forcing changes represent the largest component of the global radiative flux perturbation (RFP) differences. However, other components of the RFP differences may have a larger impact on surface temperature in some parts of the world.

The enhanced aerosol emissions in A2x lead to widespread cooling in the Northern Hemisphere,

partially offsetting greenhouse gas-induced warming. The aerosol-induced cooling is particularly strong over some land regions, including East Asia and South Asia. The cooling effect also extends to many regions in the Southern Hemisphere, including Australia. Surface temperature gradients, including the interhemispheric temperature gradient, are affected.

We have also observed that the enhanced aerosol emissions in A2x impact precipitation:

- (i) The warming-induced precipitation increase in the Northern Hemisphere tropics is partially offset. The ITCZ shifts southward, especially over the Indian Ocean, in response to changes in the interhemispheric temperature gradient.
- (ii) Over East Asia, summer monsoon precipitation is suppressed. This is associated with a weakening of the East Asian branch of the Hadley circulation. The “slow response” of SSTs does not appear to be an essential component of the precipitation suppression.
- (iii) Over South Asia, especially southern India, summer monsoon precipitation is also suppressed. Again, this is associated with a weakening of the Hadley circulation. In contrast to East Asia, the South Asian monsoon suppression appears to be strongly dependent on the SST response. Cooling of the SSTs in the Bay of Bengal and Arabian Sea likely plays an important role.
- (iv) Over Australia, austral summer monsoon precipitation is enhanced. This remote impact appears to be associated with a southward shift of the ITCZ, caused by an aerosol-induced modification of the interhemispheric temperature gradient. The SST response appears to play an important role.
- (v) Over the Sahel, West African monsoon precipitation is suppressed. This remote suppression may be associated with a weakening of the West African westerly jet (WAWJ). Although surface temperature gradients likely play a role, the mechanism by which Asian aerosol emissions may affect the WAWJ remains unclear, providing a focus for further research. The relative importance of the SST response is unclear.

In this study, we have demonstrated that aerosol emissions in Asia may significantly impact the hydrological cycle, especially monsoon systems, affecting precipitation both locally and remotely in other parts of the world. Our study indicates that energy and air quality policy in Asia, through consequent effects on aerosol emissions, can have important implications for future climatic changes both locally and globally.

Acknowledgments. This research was supported by the National Research Foundation Singapore through the Singapore–MIT Alliance for Research and Technology’s Center for Environmental Sensing and Modeling interdisciplinary research program. HC was supported through a Singapore–MIT Undergraduate Research Fellowship (SMURF). This research was also supported by the U.S. National Science Foundation (AGS-0944121), DOE (DE-FG02-94ER61937), U.S. EPA (XA-83600001-1), and the A*STAR Computational Resource Centre of Singapore (<http://www.acrc.a-star.edu.sg>) through the use of its high performance computing facilities. The authors thank Phil Rasch, Balwinder Singh, and Jin-Ho Yoon, who provided initial conditions data and provided advice on the RCP4.5 model configuration. The model data analyzed in this study are available at <http://dx.doi.org/10.6084/m9.figshare.2067084>.

APPENDIX

Notes On Analysis Methodology

a. Calculation of annual means

When calculating the annual means of the model output data, years are defined to start in December of the preceding year and finish in November. This is done so as not to divide the December–February season across two different years. For example, the 2080–99 20-yr averaging period actually covers December 2079–November 2099.

The first complete year is 2007 (December 2006–November 2007). Hence, the input for data for the time series (Figs. 3, 8, 10, and 16) starts in 2007.

b. Statistical significance testing of differences between ensembles

For a given 20-yr period, an independent two-sample *t* test is used to test whether the two ensemble means are significantly different from each other. Annual means for each individual ensemble member are used as the input data. Hence, whenever significance is tested, 60 annual means (20 yr \times 3 members per ensemble) are available for each of the RCP4.5 and A2x ensembles. It is assumed that the two ensembles have equal variance. A two-tailed *p*-value threshold of 0.05 is used. Specific details of how significance is indicated in the different types of figures is provided below.

In the time series figures (Figs. 3, 8, 10, and 16), significance is tested for each 20-yr period, starting with 2007–26, then 2008–27, etc. Significance is indicated by a green line.

In the zonal mean figures (Figs. 9 and 11), for the 20-yr period 2080–99, significance is tested at each latitude (at

the model resolution). Significance is indicated by a green line.

In the maps showing differences between the transient ensembles (Figs. 7 and 12), for the 20-yr period 2080–99, significance is tested at each grid box. Statistical significance is indicated by stippling.

In the Hovmöller diagrams (Figs. 13, 14, and 15), for the 20-yr period 2080–99, significance is tested at each latitude and month. Significance is indicated by the diagonal crosses.

c. Statistical significance testing of regression slopes

The linear regression slopes in Figs. 3, 8, 10, and 16 have been calculated using ensemble mean annual means as the input data. Autocorrelation has been accounted for when testing the statistical significance of the regression slopes. Assuming that the detrended data can be modeled as a first-order autoregressive process, autocorrelation is accounted for by replacing the sample size *n* with an effective sample size n_e :

$$n_e = \begin{cases} n, & \text{if } r_1 \leq 0 \\ n \frac{1 - r_1}{1 + r_1}, & \text{if } r_1 > 0 \end{cases}, \quad (\text{A1})$$

where r_1 is the lag-1 autocorrelation coefficient (Wilks 2006). Cases with a two-tailed *p* value >0.05 are classified as insignificant.

REFERENCES

- Ackerman, A. S., 2000: Reduction of tropical cloudiness by soot. *Science*, **288**, 1042–1047, doi:10.1126/science.288.5468.1042.
- Albrecht, B. A., 1989: Aerosols, cloud microphysics, and fractional cloudiness. *Science*, **245**, 1227–1230, doi:10.1126/science.245.4923.1227.
- Bala, G., K. Caldeira, and R. Nemani, 2010: Fast versus slow response in climate change: Implications for the global hydrological cycle. *Climate Dyn.*, **35**, 423–434, doi:10.1007/s00382-009-0583-y.
- Bollasina, M. A., Y. Ming, and V. Ramaswamy, 2011: Anthropogenic aerosols and the weakening of the South Asian summer monsoon. *Science*, **334**, 502–505, doi:10.1126/science.1204994.
- , —, —, M. D. Schwarzkopf, and V. Naik, 2014: Contribution of local and remote anthropogenic aerosols to the twentieth century weakening of the South Asian monsoon. *Geophys. Res. Lett.*, **41**, 680–687, doi:10.1002/2013GL058183.
- Booth, B. B. B., N. J. Dunstone, P. R. Halloran, T. Andrews, and N. Bellouin, 2012: Aerosols implicated as a prime driver of twentieth-century North Atlantic climate variability. *Nature*, **484**, 228–232, doi:10.1038/nature10946.
- Chiang, J. C., and A. R. Friedman, 2012: Extratropical cooling, interhemispheric thermal gradients, and tropical climate change. *Annu. Rev. Earth Planet. Sci.*, **40**, 383–412, doi:10.1146/annurev-earth-042711-105545.
- Chung, C. E., V. Ramanathan, and J. T. Kiehl, 2002: Effects of the South Asian absorbing haze on the northeast monsoon and

- surface–air heat exchange. *J. Climate*, **15**, 2462–2476, doi:10.1175/1520-0442(2002)015<2462:EOTSAA>2.0.CO;2.
- Cohen, J. B., and C. Wang, 2014: Estimating global black carbon emissions using a top-down Kalman filter approach. *J. Geophys. Res. Atmos.*, **119**, 307–323, doi:10.1002/2013JD019912.
- Cowan, T., and W. Cai, 2011: The impact of Asian and non-Asian anthropogenic aerosols on 20th century Asian summer monsoon. *Geophys. Res. Lett.*, **38**, L11703, doi:10.1029/2011GL047268.
- Dentener, F., and Coauthors, 2006: Emissions of primary aerosol and precursor gases in the years 2000 and 1750 prescribed data-sets for AeroCom. *Atmos. Chem. Phys.*, **6**, 4321–4344, doi:10.5194/acp-6-4321-2006.
- Dong, B., R. T. Sutton, E. Highwood, and L. Wilcox, 2014: The impacts of European and Asian anthropogenic sulfur dioxide emissions on Sahel rainfall. *J. Climate*, **27**, 7000–7017, doi:10.1175/JCLI-D-13-00769.1.
- Fiore, A. M., and Coauthors, 2012: Global air quality and climate. *Chem. Soc. Rev.*, **41**, 6663–6683, doi:10.1039/c2cs35095e.
- Ganguly, D., P. J. Rasch, H. Wang, and J.-H. Yoon, 2012: Climate response of the South Asian monsoon system to anthropogenic aerosols. *J. Geophys. Res.*, **117**, D13209, doi:10.1029/2012JD017508.
- Gent, P. R., and Coauthors, 2011: The Community Climate System Model version 4. *J. Climate*, **24**, 4973–4991, doi:10.1175/2011JCLI4083.1.
- Gottelman, A., and Coauthors, 2010: Global simulations of ice nucleation and ice supersaturation with an improved cloud scheme in the Community Atmosphere Model. *J. Geophys. Res.*, **115**, D18216, doi:10.1029/2009JD013797.
- , X. Liu, D. Barahona, U. Lohmann, and C. Chen, 2012: Climate impacts of ice nucleation. *J. Geophys. Res.*, **117**, D20201, doi:10.1029/2012JD017950.
- Ghan, S. J., 2013: Technical note: Estimating aerosol effects on cloud radiative forcing. *Atmos. Chem. Phys.*, **13**, 9971–9974, doi:10.5194/acp-13-9971-2013.
- , X. Liu, R. C. Easter, R. Zaveri, P. J. Rasch, J.-H. Yoon, and B. Eaton, 2012: Toward a minimal representation of aerosols in climate models: Comparative decomposition of aerosol direct, semidirect, and indirect radiative forcing. *J. Climate*, **25**, 6461–6476, doi:10.1175/JCLI-D-11-00650.1.
- Gu, Y., K. N. Liou, Y. Xue, C. R. Mechoso, W. Li, and Y. Luo, 2006: Climatic effects of different aerosol types in China simulated by the UCLA general circulation model. *J. Geophys. Res.*, **111**, D15201, doi:10.1029/2005JD006312.
- Guo, L., E. J. Highwood, L. C. Shaffrey, and G. Turner, 2013: The effect of regional changes in anthropogenic aerosols on rainfall of the East Asian summer monsoon. *Atmos. Chem. Phys.*, **13**, 1521–1534, doi:10.5194/acp-13-1521-2013.
- Haywood, J., and O. Boucher, 2000: Estimates of the direct and indirect radiative forcing due to tropospheric aerosols: A review. *Rev. Geophys.*, **38**, 513–543, doi:10.1029/1999RG000078.
- , L. Donner, A. Jones, and J.-C. Golaz, 2009: Global indirect radiative forcing caused by aerosols: IPCC (2007) and beyond. *Clouds in the Perturbed Climate System: Their Relationship to Energy Balance, Atmospheric Dynamics, and Precipitation*, J. Heintzenberg and R. Charlson, Eds., MIT Press, 451–467.
- , A. Jones, N. Bellouin, and D. Stephenson, 2013: Asymmetric forcing from stratospheric aerosols impacts Sahelian rainfall. *Nat. Climate Change*, **3**, 660–665, doi:10.1038/nclimate1857.
- Held, I. M., and B. J. Soden, 2006: Robust responses of the hydrological cycle to global warming. *J. Climate*, **19**, 5686–5699, doi:10.1175/JCLI3990.1.
- Jiang, Y., X. Liu, X.-Q. Yang, and M. Wang, 2013: A numerical study of the effect of different aerosol types on East Asian summer clouds and precipitation. *Atmos. Environ.*, **70**, 51–63, doi:10.1016/j.atmosenv.2012.12.039.
- Lamarque, J.-F., G. P. Kyle, M. Meinshausen, K. Riahi, S. J. Smith, D. P. van Vuuren, A. J. Conley, and F. Vitt, 2011: Global and regional evolution of short-lived radiatively active gases and aerosols in the representative concentration pathways. *Climatic Change*, **109**, 191–212, doi:10.1007/s10584-011-0155-0.
- Lau, K. M., M. K. Kim, and K. M. Kim, 2006: Asian summer monsoon anomalies induced by aerosol direct forcing: The role of the Tibetan Plateau. *Climate Dyn.*, **26**, 855–864, doi:10.1007/s00382-006-0114-z.
- Lee, S.-Y., and C. Wang, 2015: The response of the South Asian summer monsoon to temporal and spatial variations in absorbing aerosol radiative forcing. *J. Climate*, **28**, 6626–6646, doi:10.1175/JCLI-D-14-00609.1.
- , H.-J. Shin, and C. Wang, 2013: Nonlinear effects of coexisting surface and atmospheric forcing of anthropogenic absorbing aerosols: Impact on the South Asian monsoon onset. *J. Climate*, **26**, 5594–5607, doi:10.1175/JCLI-D-12-00741.1.
- Levy, H., L. W. Horowitz, M. D. Schwarzkopf, Y. Ming, J.-C. Golaz, V. Naik, and V. Ramaswamy, 2013: The roles of aerosol direct and indirect effects in past and future climate change. *J. Geophys. Res. Atmos.*, **118**, 4521–4532, doi:10.1002/jgrd.50192.
- Liu, X., X. Xie, Z.-Y. Yin, C. Liu, and A. Gottelman, 2011: A modeling study of the effects of aerosols on clouds and precipitation over East Asia. *Theor. Appl. Climatol.*, **106**, 343–354, doi:10.1007/s00704-011-0436-6.
- , and Coauthors, 2012: Toward a minimal representation of aerosols in climate models: Description and evaluation in the Community Atmosphere Model CAM5. *Geosci. Model Dev.*, **5**, 709–739, doi:10.5194/gmd-5-709-2012.
- Lu, Z., Q. Zhang, and D. G. Streets, 2011: Sulfur dioxide and primary carbonaceous aerosol emissions in China and India, 1996–2010. *Atmos. Chem. Phys.*, **11**, 9839–9864, doi:10.5194/acp-11-9839-2011.
- Meehl, G. A., J. M. Arblaster, and W. D. Collins, 2008: Effects of black carbon aerosols on the Indian monsoon. *J. Climate*, **21**, 2869–2882, doi:10.1175/2007JCLI1777.1.
- , and Coauthors, 2013: Climate change projections in CESM1 (CAM5) compared to CCSM4. *J. Climate*, **26**, 6287–6308, doi:10.1175/JCLI-D-12-00572.1.
- Menon, S., J. Hansen, L. Nazarenko, and Y. Luo, 2002: Climate effects of black carbon aerosols in China and India. *Science*, **297**, 2250–2253, doi:10.1126/science.1075159.
- Morrison, H., and A. Gottelman, 2008: A new two-moment bulk stratiform cloud microphysics scheme in the Community Atmosphere Model, version 3 (CAM3). Part I: Description and numerical tests. *J. Climate*, **21**, 3642–3659, doi:10.1175/2008JCLI2105.1.
- Neale, R. B., and Coauthors, 2012: Description of the NCAR Community Atmosphere Model (CAM 5.0). NCAR Tech. Note TN-486+STR, 274 pp. [Available online at http://www.cesm.ucar.edu/models/cesm1.0/cam/docs/description/cam5_desc.pdf.]
- Pithan, F., and T. Mauritsen, 2014: Arctic amplification dominated by temperature feedbacks in contemporary climate models. *Nat. Geosci.*, **7**, 181–184, doi:10.1038/ngeo2071.
- Pu, B., and K. H. Cook, 2012: Role of the West African westerly jet in Sahel rainfall variations. *J. Climate*, **25**, 2880–2896, doi:10.1175/JCLI-D-11-00394.1.
- Ramanathan, V., and Coauthors, 2005: Atmospheric brown clouds: Impacts on South Asian climate and hydrological cycle. *Proc.*

- Natl. Acad. Sci. USA*, **102**, 5326–5333, doi:10.1073/pnas.0500656102.
- Rotstayn, L. D., S. J. Jeffrey, M. A. Collier, S. M. Dravitzki, A. C. Hirst, J. I. Syktus, and K. K. Wong, 2012: Aerosol- and greenhouse gas-induced changes in summer rainfall and circulation in the Australasian region: A study using single-forcing climate simulations. *Atmos. Chem. Phys.*, **12**, 6377–6404, doi:10.5194/acp-12-6377-2012.
- , M. A. Collier, A. Chrastansky, S. J. Jeffrey, and J.-J. Luo, 2013: Projected effects of declining aerosols in RCP4.5: Unmasking global warming? *Atmos. Chem. Phys.*, **13**, 10883–10905, doi:10.5194/acp-13-10883-2013.
- Shindell, D. T., and Coauthors, 2013: Radiative forcing in the ACCMIP historical and future climate simulations. *Atmos. Chem. Phys.*, **13**, 2939–2974, doi:10.5194/acp-13-2939-2013.
- Steckel, J. C., O. Edenhofer, and M. Jakob, 2015: Drivers for the renaissance of coal. *Proc. Natl. Acad. Sci. USA*, **112**, E3775–E3781, doi:10.1073/pnas.1422722112.
- Stevens, B., and G. Feingold, 2009: Untangling aerosol effects on clouds and precipitation in a buffered system. *Nature*, **461**, 607–613, doi:10.1038/nature08281.
- Tao, W. K., J. P. Chen, Z. Li, C. Wang, and C. Zhang, 2012: Impact of aerosols on convective clouds and precipitation. *Rev. Geophys.*, **50**, RG2001, doi:10.1029/2011RG000369.
- Teng, H., W. M. Washington, G. Branstator, G. A. Meehl, and J.-F. Lamarque, 2012: Potential impacts of Asian carbon aerosols on future US warming. *Geophys. Res. Lett.*, **39**, L11703, doi:10.1029/2012GL051723.
- Twomey, S., 1974: Pollution and the planetary albedo. *Atmos. Environ.*, **8**, 1251–1256, doi:10.1016/0004-6981(74)90004-3.
- , 1977: The influence of pollution on the shortwave albedo of clouds. *J. Atmos. Sci.*, **34**, 1149–1152, doi:10.1175/1520-0469(1977)034<1149:TIPOT>2.0.CO;2.
- U.S. Energy Information Administration, 2013: Technically Recoverable Shale Oil And Shale Gas Resources: An assessment of 137 shale formations in 41 countries outside the United States. Accessed 16 October 2013. [Available online at <http://www.eia.gov/analysis/studies/worldshalegas/>.]
- van Vuuren, D. P., and Coauthors, 2011: The representative concentration pathways: An overview. *Climatic Change*, **109**, 5–31, doi:10.1007/s10584-011-0148-z.
- Wang, C., 2004: A modeling study on the climate impacts of black carbon aerosols. *J. Geophys. Res.*, **109**, D03106, doi:10.1029/2003JD004084.
- , 2007: Impact of direct radiative forcing of black carbon aerosols on tropical convective precipitation. *Geophys. Res. Lett.*, **34**, L05709, doi:10.1029/2006GL028416.
- , 2009: The sensitivity of tropical convective precipitation to the direct radiative forcings of black carbon aerosols emitted from major regions. *Ann. Geophys.*, **27**, 3705–3711, doi:10.5194/angeo-27-3705-2009.
- , 2013: Impact of anthropogenic absorbing aerosols on clouds and precipitation: A review of recent progresses. *Atmos. Res.*, **122**, 237–249, doi:10.1016/j.atmosres.2012.11.005.
- , 2015: Anthropogenic aerosols and the distribution of past large-scale precipitation change. *Geophys. Res. Lett.*, **42**, 10876–10884, doi:10.1002/2015GL066416.
- , D. Kim, A. M. L. Ekman, M. C. Barth, and P. J. Rasch, 2009: Impact of anthropogenic aerosols on Indian summer monsoon. *Geophys. Res. Lett.*, **36**, L21704, doi:10.1029/2009GL040114.
- Wilks, D. S., 2006: *Statistical Methods in the Atmospheric Sciences*. 2nd ed. Academic Press, 627 pp.
- Zhao, Y., S. Wang, C. P. Nielsen, X. Li, and J. Hao, 2010: Establishment of a database of emission factors for atmospheric pollutants from Chinese coal-fired power plants. *Atmos. Environ.*, **44**, 1515–1523, doi:10.1016/j.atmosenv.2010.01.017.
- Zhi, G., C. Peng, Y. Chen, D. Liu, G. Sheng, and J. Fu, 2009: Deployment of coal briquettes and improved stoves: Possibly an option for both environment and climate. *Environ. Sci. Technol.*, **43**, 5586–5591, doi:10.1021/es802955d.

Joint Program Reprint Series - Recent Articles

For limited quantities, Joint Program publications are available free of charge. Contact the Joint Program office to order.

Complete list: <http://globalchange.mit.edu/publications>

- 2016-8 Transient Climate Impacts for Scenarios of Aerosol Emissions from Asia: A Story of Coal versus Gas.** Grandey, B.S., H. Cheng and C. Wang, *Journal of Climate*, 29(8): 2849–2867 (2016)
- 2016-7 Climate and Land: Tradeoffs and Opportunities.** Reilly, J.M. and J.M. Melillo, *Geoinformatics & Geostatistics: An Overview*, 4(1): 1000135 (2016)
- 2016-6 Projections of Water Stress Based on an Ensemble of Socioeconomic Growth and Climate Change Scenarios: A Case Study in Asia.** Fant, C., C.A. Schlosser, X. Gao, K. Strzepek and J. Reilly, *PLoS ONE* 11(3): e0150633 (2016)
- 2016-5 Determinants of Crop Yield and Profit of Family Farms: Evidence from the Senegal River Valley.** Blanc, É., A. Lépine and E. Strobl, *Experimental Agriculture*, 52(1): 110–136 (2016)
- 2016-4 Metamodeling of Droplet Activation for Global Climate Models.** Rothenberg, D. and C. Wang, *Journal of the Atmospheric Sciences*, 73, 1255–1272 (2016)
- 2016-3 Climate extremes and ozone pollution: a growing threat to China's food security.** Tian, H., W. Ren, B. Tao, G. Sun, A. Chappelka, X. Wang, S. Pan, J. Yang, J. Liu, B.S. Felzer, J.M. Melillo and J. Reilly, *Ecosystem Health and Sustainability*, 2(1): 2332–8878 (2016)
- 2016-2 Carbon emissions in China: How far can new efforts bend the curve?** Zhang, X., V.J. Karplus, T. Qi, D. Zhang and J. He, *Energy Economics*, 54 (Feb 2016): 388–395 (2016)
- 2016-1 Long-term economic modeling for climate change assessment.** Y.-H.H. Chen, S. Paltsev, J.M. Reilly, J.F. Morris and M.H. Babiker, *Economic Modelling*, 52(Part B): 867–883 (2016)
- 2015-33 The Response of the South Asian Summer Monsoon to Temporal and Spatial Variations in Absorbing Aerosol Radiative Forcing.** Lee, S.-Y. and C. Wang, *Journal of Climate*, 28, 6626–6646 (2016)
- 2015-32 The Observed State of the Water Cycle in the Early Twenty-First Century.** Rodell, M., H.K. Beaudoin, T.S. L'Ecuyer, W.S. Olson, J.S. Famiglietti, P.R. Houser, R. Adler, M.G. Bosilovich, C.A. Clayson, D. Chambers, E. Clark, E.J. Fetzer, X. Gao, G. Gu, K. Hilburn, G.J. Huffman, D.P. Lettenmaier, W.T. Liu, F.R. Robertson, C.A. Schlosser, J. Sheffield, and E.F. Wood, *Journal of Climate*, 28, 8289–8318 (2016)
- 2015-31 Anthropogenic aerosols and the distribution of past large-scale precipitation change.** Wang, C., *Geophysical Research Letters*, 42, 10,876–10,884 (2015)
- 2015-30 Consumption-Based Adjustment of Emissions-Intensity Targets: An Economic Analysis for China's Provinces.** Springmann, M., D. Zhang and V.J. Karplus, *Environmental and Resource Economics*, 61(4): 615–640 (2014)
- 2015-29 Emulating maize yields from global gridded crop models using statistical estimates.** Blanc, É and B. Sultan, *Agricultural and Forest Meteorology*, 214-215: 134–147 (2015)
- 2015-28 Reconciling reported and unreported HFC emissions with atmospheric observations.** Lunt, M.F., M. Rigby, A.L. Ganesan, A.J. Manning, R.G. Prinn, S. O'Doherty, J. Mühle, C.M. Harth, P.K. Salameh, T. Arnold, R.F. Weiss, T. Saito, Y. Yokouchi, P.B. Krummel, L.P. Steele, P.J. Fraser, S. Li, S. Park, S. Reimann, M.K. Vollmer, C. Lunder, O. Hermansen, N. Schmidbauer, M. Maione, J. Arduini, D. Young and P.G. Simmonds, *PNAS*, 112(19): 5927–5931 (2015)
- 2015-27 The Observed State of the Energy Budget in the Early 21st Century.** L'Ecuyer, T.S., H.K. Beaudoin, M. Rodell, W. Olson, B. Lin, S. Kato, C.A. Clayson, E. Wood, J. Sheffield, R. Adler, G. Huffman, M. Bosilovich, G. Gu, F. Robertson, P.R. Houser, D. Chambers, J.S. Famiglietti, E. Fetzer, W.T. Liu, X. Gao, C.A. Schlosser, E. Clark, D.P. Lettenmaier and K. Hilburn, *J. Climate*, 28, 8319–8346 (2015)
- 2015-26 US major crops' uncertain climate change risks and greenhouse gas mitigation benefits.** Sue Wing, I., E. Monier, A. Stern and A. Mundra, *Environmental Research Letters*, 10(2015): 115002 (2015)
- 2015-25 Benefits of mercury controls for the United States.** Giang, A. and N.E. Selin, *PNAS*, online first (doi: 10.1073/pnas.1514395113) (2015)
- 2015-24 Electricity generation costs of concentrated solar power technologies in China based on operational plants.** Zhu, Z., D. Zhang, P. Mischke and X. Zhang, *Energy*, 89(September): 65–74 (2015)
- 2015-23 An analysis of China's climate policy using the China-Global Energy Model.** Qi, T., N. Winchester, V.J. Karplus, D. Zhang and X. Zhang, *Economic Modelling*, 52(Part B): 650–660 (2015).
- 2015-22 Protected areas' role in climate-change mitigation.** Melillo, J.M., X. Lu, D.W. Kicklighter, J.M. Reilly, Y. Cai and A.P. Sokolov, *Ambio*, online first (doi: 10.1007/s13280-015-0693-1)
- 2015-21 The impact of climate change on wind and solar resources in southern Africa.** Fant, C., C.A. Schlosser and K. Strzepek, *Applied Energy* 161, online first (doi: 10.1016/j.apenergy.2015.03.042) (2015)
- 2015-20 Enhanced marine sulphur emissions offset global warming and impact rainfall.** Grandey, B.S. and C. Wang, *Scientific Reports* 5 (Article: 13055) (2015)
- 2015-19 Climate change impacts and greenhouse gas mitigation effects on U.S. water quality.** Boehlert, B., K.M. Strzepek, S.C. Chapra, C. Fant, Y. Gebretsadik, M. Lickley, R. Swanson, A. McCluskey, J.E. Neumann and J. Martinich, *Journal of Advances in Modeling Earth Systems* 7(3): 1326–1338 (2015)